

# Evaluation of archived and off-line diagnosed vertical diffusion coefficients from ERA-40 with $^{222}\text{Rn}$ simulations

D. J. L. Olivie<sup>1,2</sup>, P. F. J. van Velthoven<sup>1</sup>, and A. C. M. Beljaars<sup>3</sup>

<sup>1</sup>Royal Netherlands Meteorological Institute, De Bilt, The Netherlands

<sup>2</sup>Eindhoven University of Technology, Eindhoven, The Netherlands

<sup>3</sup>European Centre for Medium-range Weather Forecasts, Reading, UK

Received: 15 June 2004 – Published in Atmos. Chem. Phys. Discuss.: 3 August 2004

Revised: 2 November 2004 – Accepted: 11 November 2004 – Published: 26 November 2004

**Abstract.** Boundary layer turbulence has a profound influence on the distribution of tracers with sources or sinks at the surface. The 40-year ERA-40 meteorological data set of the European Centre for Medium-range Weather Forecasts contains archived vertical diffusion coefficients. We evaluated the use of these archived diffusion coefficients versus off-line diagnosed coefficients based on other meteorological parameters archived during ERA-40 by examining the influence on the distribution of the radionuclide  $^{222}\text{Rn}$  in the chemistry transport model TM3. In total four different sets of vertical diffusion coefficients are compared: (i) 3-hourly vertical diffusion coefficients archived during the ERA-40 project, (ii) 3-hourly off-line diagnosed coefficients from a non-local scheme based on Holtslag and Boville (1993), Vogelesang and Holtslag (1996), and Beljaars and Viterbo (1999), (iii) 6-hourly coefficients archived during the ERA-40 project, and (iv) 6-hourly off-line diagnosed coefficients based on a local scheme described in Louis (1979) and Louis et al. (1982). The diffusion scheme to diagnose the coefficients off-line in (ii) is similar to the diffusion scheme used during the ERA-40 project (i and iii).

The archived diffusion coefficients from the ERA-40 project which are time-averaged cause stronger mixing than the instantaneous off-line diagnosed diffusion coefficients. This can be partially attributed to the effect of instantaneous versus time-averaged coefficients, as well as to differences in the diffusion schemes. The 3-hourly off-line diagnosis of diffusion coefficients can reproduce quite well the 3-hourly archived diffusion coefficients.

Atmospheric boundary layer heights of the sets (ii) and (iii) are also compared. Both were found to be in reasonable agreement with observations of the atmospheric boundary layer height in Cabauw (the Netherlands) and from the FIFE-campaign (United States) during summer.

Correspondence to: D. J. L. Olivie  
(olivie@knmi.nl)

Simulations of  $^{222}\text{Rn}$  with the TM3 model using these four sets of vertical diffusion coefficients are compared to surface measurements of  $^{222}\text{Rn}$  at the mid-latitude continental stations Freiburg, Schauinsland, Cincinnati and Socorro in order to evaluate the effect of these different sets of diffusion coefficients on the tracer transport. It is found that the daily cycle of the  $^{222}\text{Rn}$  concentration is well represented using 3-hourly diffusion coefficients. Comparison with observations of  $^{222}\text{Rn}$  data with the station in Schauinsland which is situated on a hill shows that all considered schemes underestimate the amplitude of the daily cycle of the  $^{222}\text{Rn}$  concentration in the upper part of the atmospheric boundary layer.

## 1 Introduction

Boundary layer turbulence is an important transport mechanism in the troposphere (Wang et al., 1999). In the convective or turbulent atmospheric boundary layer (ABL) tracers can be transported throughout the height range of the ABL in time intervals of tens of minutes. All species emitted at the surface must pass through the ABL in order to reach the free troposphere. Because turbulence acts on spatial scales that are much smaller than the typical size of the grid cells of global atmospheric models, turbulent diffusion must be parameterised in these models.

The European Centre for Medium-range Weather Forecasts (ECMWF) re-analysis project (ERA-40) aims at providing a consistent time series of the state of the global atmosphere for the period 1957–2002 (Simmons and Gibson, 2000). A wide variety of meteorological fields were archived in ERA-40. In the earlier ERA-15 re-analysis project (Gibson et al., 1997) where the atmosphere for the period 1979–1993 has been reanalysed, meteorological fields describing small-scale transport like convection or boundary layer turbulence were not archived. The more recent ERA-40 data set is one of the first long-term meteorological data sets where

vertical diffusion coefficients for heat are archived (available as 3- or 6-hourly averaged values).

Meteorological data sets such as ERA-40 and ERA-15 are commonly used to study the transport and chemical evolution of atmospheric gases and aerosols in chemical transport models (CTMs). The chemical transport model TM3 (Tracer Model Version 3) is a global atmospheric model, which is applied to evaluate the atmospheric composition, and changes herein caused by natural and anthropogenic changes. For describing the turbulent transport, it can use different turbulent diffusion data. Until now, two off-line vertical diffusion schemes have been used in the TM3 model, where the diffusion coefficients are diagnosed off-line based on other regularly (e.g. 6-hourly) archived meteorological fields. The first scheme, based on Louis (1979) and Louis et al. (1982), is a local diffusion scheme that describes the vertical diffusion coefficient as a function of a mixing length scale, the local gradient of the wind, and the virtual temperature. However, under convective conditions, when the largest transporting eddies may have sizes similar to the depth of the ABL, local schemes do not perform well (Troen and Mahrt, 1986): the characteristics of the large eddies are not properly taken into account. The second scheme, based on a combination of Holtslag and Boville (1993), Voegelehang and Holtslag (1996) and Beljaars and Viterbo (1999), is a non-local diffusion scheme. Non-local ABL schemes often contain a term that describes counter gradient transport by the large eddies (Troen and Mahrt, 1986), and prescribe the shape of the vertical profile of the diffusion coefficient. Apart from the meteorological fields needed for a local scheme, a non-local scheme also uses the surface sensible and latent heat fluxes. The vertical exchange has been shown to be more pronounced with non-local schemes than with local schemes (Holtslag and Boville, 1993; Holtslag et al., 1995). The 3-hourly off-line scheme (Holtslag and Boville, 1993; Voegelehang and Holtslag, 1996; Beljaars and Viterbo, 1999) is currently most used in the TM3 model. The 6-hourly off-line scheme (Louis, 1979; Louis et al., 1982) was until recently used in the TM3 model for various studies: Dentener et al. (2003) used meteorological data from the ERA-15 project (which does not provide 3-hourly surface latent heat fluxes) and the 6-hourly off-line scheme (Louis, 1979; Louis et al., 1982). From now on however, the ERA-40 data set allows the use of archived vertical diffusion data (3-hourly or 6-hourly) in the TM3 model. One of the first to use archived sub-grid meteorological parameters was Allen et al. (1996). They used archived convective mass fluxes and detrainments, as well as the ABL heights. An advantage of the use of archived meteorological fields to describe small-scale transport in CTMs, is the consistency of these fields with the archived fields of cloud cover, temperature, humidity or precipitation.

The effect on the transport of tracers by the diffusion data can be studied by making  $^{222}\text{Rn}$  simulations with CTMs.  $^{222}\text{Rn}$  is an excellent tracer to study the transport character-

istics on short time scales (hours to weeks) because it has an almost uniform emission rate over land and is only lost through radioactive decay with an e-folding lifetime of about 5.5 days (Dentener et al., 1999; Balkanski and Jacob, 1990; Kritz et al., 1990; Brost and Chatfield, 1989; Polian et al., 1986). Therefore  $^{222}\text{Rn}$  has been used extensively to evaluate parameterisations of convective transport (Mahowald et al., 1997; Allen et al., 1996; Feichter and Crutzen, 1990; Jacob and Prather, 1990) and ABL diffusion (Stockwell and Chipperfield, 1999; Stockwell et al., 1998; Jacob et al., 1997; Lee and Larsen, 1997; Mahowald et al., 1997) in atmospheric models.

In this work, we try to answer the following questions: (1) How well is the mid-latitude summer time ABL height reproduced in the ERA-40 data and in an off-line model driven by ERA-40 data? (2a) Can diffusion coefficients be reproduced accurately off-line for use in CTMs? (2b) How do local ABL schemes perform versus non-local ABL schemes when applied off-line? (3a) How crucial is a 3-hourly time resolution for diffusion data for CTM-modelling? (3b) What is the influence of using time-averaged diffusion coefficients on the tracer transport in CTMs?

To answer these questions, we will start with a description of the TM3 model and the diffusion schemes that generate the different sets of vertical diffusion coefficients (Sect. 2). In that section we will also describe the  $^{222}\text{Rn}$  emission scenario in the TM3 model, the  $^{222}\text{Rn}$  observations, and the ABL height observations. In Sect. 3 we will first compare the vertical diffusion coefficients from the different schemes. Then we will compare the modelled ABL height at two mid-latitude stations with observations. Next we will compare the  $^{222}\text{Rn}$  concentration which is modelled in the TM3 model using the different sets of diffusion data, with surface measurements of the  $^{222}\text{Rn}$  concentration at four selected surface stations. In Sect. 4 we will formulate the conclusions and formulate some recommendations.

## 2 Methods

### 2.1 The TM3 chemistry transport model

The chemical transport model TM3 (Tracer Model Version 3) is a global atmospheric CTM with a regular longitude-latitude grid and hybrid  $\sigma$ -pressure levels (Lelieveld and Dentener, 2000; Houweling et al., 1998; Heimann, 1995). The meteorological input data for TM3 from ERA-40 is available for 1957 to 2002. For dynamics calculations ERA-40 used a spectral truncation of T159. The physical calculations were done on a reduced Gaussian grid of 160 nodes (N80). In the vertical, 60 hybrid  $\sigma$ -pressure levels (Simmons and Burridge, 1981) were used, reaching up to 0.1 hPa. To be used in the TM3 model, the meteorological data is interpolated or averaged to the desired TM3 grid cells (Bregman et al., 2003). For advection of the tracers,

the model uses the slopes scheme developed by Russel and Lerner (Russell and Lerner, 1981). To describe the effect of convective transport on the tracer concentration, we used the archived convective mass fluxes from the ERA-40 data set (Olivie et al., 2004). The convection scheme in the ECMWF-model used during the ERA-40 project is based on Tiedtke (1989), Gregory et al. (2000), and Nordeng (1994).

The vertical diffusion of tracers in the TM3 model is described with a first order closure scheme. The net turbulent tracer flux  $\overline{w'\chi'}$  is expressed as

$$-\overline{w'\chi'} = K_z \frac{\partial \chi}{\partial z}, \quad (1)$$

where  $K_z$  is the vertical diffusion coefficient for heat,  $w$  the vertical velocity,  $\chi$  the tracer concentration, and  $z$  the height above the surface. It is assumed that the vertical diffusion coefficient for tracers is equal to the vertical diffusion coefficient for heat. In contrast to Holtslag and Boville (1993) and Wang et al. (1999), there is no counter gradient term in the TM3 implementation.

The vertical diffusion coefficients are applied in the TM3 model by converting the vertical diffusion coefficients into upward and downward vertical air mass fluxes of equal magnitude which model the exchange between two model layers. These air mass fluxes are combined with the vertical convective mass fluxes from the convection parameterisation to calculate the sub-grid scale vertical tracer transport with an implicit numerical scheme. This allows the time steps in the TM3 model to be rather large, without introducing stability problems. In the case of very large time steps, the effect of the scheme is that it pushes the tracer concentration at once to its equilibrium distribution. In this study, we used a time step of 1 h for the small-scale vertical transport.

From Eq. (1) one derives that the dimensions of  $K_z$  are  $L^2T^{-1}$ . Taking the ABL height as a representative length scale for the effect of diffusion gives a relationship between  $K_z$  and the time scale of turbulent diffusion. If for example the ABL height is 1000 m and  $K_z$  is 300  $m^2/s$ , one finds a time scale of around 1 h. This means that a tracer initially only present at the surface, will be well mixed throughout the complete ABL on a time scale of 1 h.

## 2.2 Vertical diffusion data

Different sets of vertical diffusion coefficients are used in the TM3 model. We will briefly describe the schemes that are used to calculate these data sets.

### 2.2.1 The ERA-40 3-hourly and 6-hourly diffusion coefficients

The scheme as it is used in the ERA-40 project is described in the documentation of the cycle CY23r4 of the ECMWF model, see <http://www.ecmwf.int/research/ifsdocs/CY23r4/>. It is a non-local scheme. The coefficients for vertical dif-

fusion of heat were stored during the ERA-40 project as 3-hourly averaged values. They can also be combined to 6-hourly averaged values.

Different formulations are used based on the stability regime that is determined by the virtual potential temperature flux  $\overline{(w'\theta'_v)_0}$ . If the surface layer is unstable ( $\overline{(w'\theta'_v)_0} > 0$ ), then a method according to Troen and Mahrt (1986) is applied. This method determines the ABL height  $h$  using a parcel method where the parcel is lifted from the minimum virtual temperature, rather than from the surface. The dimensionless coefficient for the excess of the parcel temperature is reduced from 6.5 (Troen and Mahrt, 1986) or 8.5 (Holtslag and Boville, 1993) to 2 (to get a well controlled entrainment rate and a less aggressive erosion of inversions). In the ABL, the vertical profile of diffusion coefficients is predefined (Troen and Mahrt, 1986)

$$K_z = \kappa w_h z \left(1 - \frac{z}{h}\right)^2, \quad (2)$$

where  $w_h$  is a turbulent velocity scale and  $\kappa=0.4$  the Von Karman constant. At the top of the ABL, there is an explicit entrainment formulation in the capping inversion. The virtual heat flux at the top of the ABL is taken proportional to the surface virtual heat flux

$$\overline{(w'\theta'_v)_h} = -C \overline{(w'\theta'_v)_0}, \quad (3)$$

with  $C=0.2$  and  $\theta_v$  the virtual potential temperature. Knowing the flux, the diffusion coefficient at the top of the ABL can be expressed as

$$K_z = C \frac{\overline{(w'\theta'_v)_0}}{\frac{\partial \theta_v}{\partial z}}, \quad (4)$$

where  $\frac{\partial \theta_v}{\partial z}$  is the virtual potential temperature gradient in the inversion layer.

If the surface layer is stable ( $\overline{(w'\theta'_v)_0} < 0$ ), the diffusion coefficients are determined by the gradient Richardson number  $Ri$  which is defined as

$$Ri = \frac{g}{\theta} \frac{\frac{\partial \theta}{\partial z}}{\left|\frac{\partial \mathbf{v}}{\partial z}\right|^2}, \quad (5)$$

where  $\mathbf{v}$  is the horizontal wind velocity. When the atmosphere is locally unstable ( $Ri < 0$ ) then

$$K_z = \frac{l_h^2}{\Phi_m \Phi_h} \left|\frac{\partial \mathbf{v}}{\partial z}\right|, \quad (6)$$

where

$$\Phi_m(\zeta) = (1 - 16\zeta)^{-\frac{1}{4}}, \quad (7)$$

and where

$$\Phi_h(\zeta) = (1 - 16\zeta)^{-\frac{1}{2}}, \quad (8)$$

where  $\zeta$  is taken equal to  $Ri$ . The mixing length  $l_h$  is calculated according to

$$\frac{1}{l_h} = \frac{1}{\kappa z} + \frac{1}{\lambda_h}. \quad (9)$$

The asymptotic mixing length  $\lambda_h$  [m] is defined as

$$\lambda_h = 30 + \frac{120}{1 + \left(\frac{z}{4000}\right)^2}, \quad (10)$$

where  $z$  [m] is the height above the surface. The asymptotic mixing length  $\lambda_h$  is a typical length scale in a neutral atmosphere for the vertical exchange of some quantity (momentum, heat, or tracer) due to turbulent eddies. In the lowest layers of the atmosphere, the size of the turbulent eddies is limited by the presence of the earth's surface, which is taken into account in the mixing length  $l_h$  in Eq. (9).

When the atmosphere is locally stable ( $Ri > 0$ ),  $\zeta$  is read from a table ( $\zeta = \zeta(Ri)$ ). The diffusion coefficients are calculated with

$$K_z = l_h^2 \left| \frac{\partial v}{\partial z} \right| F_h(Ri), \quad (11)$$

where the stability function  $F_h(Ri)$  is a revised function of the Louis et al. (1982) function (Beljaars and Viterbo, 1999)

$$F_h(Ri) = \frac{1}{1 + 2b Ri \sqrt{1 + d Ri}}, \quad (12)$$

where  $b=5$  and  $d=1$ . This formulation has less discrepancy between momentum and heat diffusion: the ratio of momentum and heat diffusion is reduced (Viterbo et al., 1999). The formulation of  $K_z$  in case of a stable surface layer also applies to the formulation of  $K_z$  above the ABL in case of an unstable surface layer.

The calculation of the atmospheric boundary layer height stored during the ERA-40 project is also described in the information about the cycle CY23r4. As well in the stable, in the neutral, as in the unstable case, a parcel lifting method proposed by Troen and Mahrt (1986) is used. They use a critical bulk Richardson number  $Ri_b=0.25$ . The bulk Richardson number is based on the difference between quantities at the level of interest and the lowest model level. This ABL height is available every 3 h and represents an instantaneous value. We only studied the 6-hourly values. We will refer to these 3-hourly diffusion coefficients as E3, and to these 6-hourly diffusion coefficients and 6-hourly ABL heights as E6.

### 2.2.2 The TM3 off-line 3-hourly and 6-hourly diffusion coefficients

The first set of off-line diagnosed diffusion coefficients in TM3 is calculated with a scheme that is rather similar to the above-described scheme. It is a non-local scheme based on Holtslag and Boville (1993), Vogelezang and Holtslag

(1996), and Beljaars and Viterbo (1999). The diffusion coefficients are calculated every 3 h, based on 3-hourly latent and sensible heat fluxes and 6-hourly fields of wind, temperature, and humidity. It has been implemented and tested in the TM3 model (Jeuken, 2000; Jeuken et al., 2001). The calculated  $K_z$  values are instantaneous values.

Although the scheme is rather similar to the aforementioned E3/E6 scheme, there are some differences: (i) a bulk Richardson criterion instead of a parcel ascent method is used to determine the height of the ABL; (ii) there is no entrainment formulation at the top of the ABL; (iii) the temperature excess of the large eddies under convective conditions is larger; (iv) the prescribed profile of the asymptotic mixing length is different; and (v) the stability functions are different.

If the surface layer is unstable ( $(\overline{w'\theta'_v})_0 > 0$ ), a prescribed profile of the vertical diffusion coefficients as in Eq. (2) is used. According to Vogelezang and Holtslag (1996) the ABL height  $h$  is the layer where the bulk Richardson number

$$Ri_b = \frac{\frac{g}{\theta_{vs}} (\theta_{vh} - \theta_{vs})(h - z_s)}{|\mathbf{v}_h - \mathbf{v}_s|^2 + b u_*^2} \quad (13)$$

reaches a critical value  $Ri_b=0.3$  (in Vogelezang and Holtslag (1996), the critical value is  $Ri_b=0.25$ ). The index  $s$  refers to values in the lowest model layer, the index  $h$  refers to values at the top of the ABL.  $u_*$  is the friction velocity. The value for  $b=100$ . The exact ABL height is calculated by linear interpolation. The temperature excess under convective conditions is calculated using a coefficient with value 8.5 (versus 2 in the E3/E6 case).

If the surface layer is stable ( $(\overline{w'\theta'_v})_0 < 0$ ), the diffusion coefficients are calculated with Eq. (11). When the atmosphere is locally stable ( $Ri > 0$ ), we take

$$F_h(Ri) = \frac{1}{1 + 10 Ri \sqrt{1 + Ri}}, \quad (14)$$

while when the atmosphere is locally unstable ( $Ri < 0$ ), we take

$$F(Ri) = 1. \quad (15)$$

Above the ABL, a formulation according to the Louis (1979) scheme is used. In the free atmosphere the stability functions in the unstable case ( $Ri < 0$ ) (Williamson et al., 1987; Holtslag and Boville, 1993) is

$$F_h(Ri) = \sqrt{1 - 18 Ri}, \quad (16)$$

and in the stable case ( $Ri > 0$ ) (Holtslag and Boville, 1993)

$$F_h(Ri) = \frac{1}{1 + 10 Ri(1 + 8 Ri)}. \quad (17)$$

The asymptotic mixing length  $\lambda_h$  [m] in this scheme is defined as

$$\lambda_h = \begin{cases} 300 & \text{if } z < 1000 \text{ m} \\ 30 + 270 \exp\left(1 - \frac{z}{1000}\right) & \text{if } z \geq 1000 \text{ m.} \end{cases} \quad (18)$$

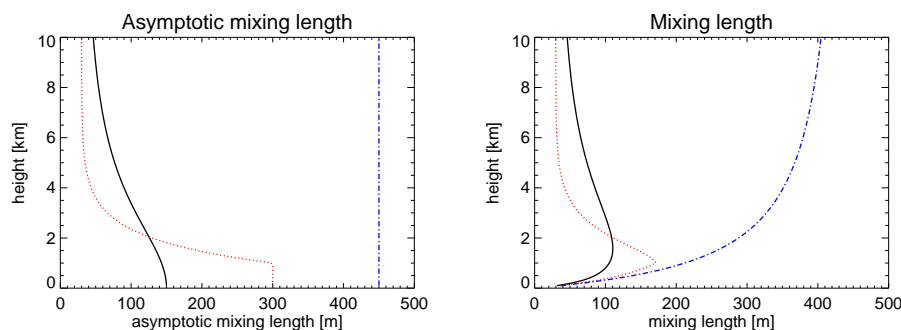


**Fig. 1.** Vertical profiles of the asymptotic mixing length (left) and mixing length (right) for heat in the different diffusion schemes: E3/E6 scheme (solid black line), H3 scheme (dotted red line), and L6 scheme (dot-dashed blue line). The mixing length can be derived from the asymptotic mixing length using Eq. (9).

We will refer to the diffusion coefficients calculated with this diffusion scheme as H3.

The second set of diffusion coefficients that are off-line diagnosed in TM3 is based on a local diffusion scheme described in Louis (1979) and Louis et al. (1982). These fields of vertical diffusion coefficients are calculated every 6 h, based on 6-hourly fields of wind, temperature, and humidity. The vertical diffusion coefficients are expressed as in Eq. (11). The stability function  $F_h(Ri)$  in the stable case ( $Ri > 0$ ) is

$$F_h(Ri) = \frac{1}{1 + 3b Ri \sqrt{1 + d Ri}}, \quad (19)$$

where  $b=5$  and  $d=5$ , and in the unstable case ( $Ri < 0$ )

$$F_h(Ri) = 1 - \frac{3b Ri}{1 + 3bc l^2 \sqrt{-\frac{Ri}{2} \left[ \frac{\left(1 + \frac{\Delta z}{z}\right)^{\frac{1}{3}} - 1}{\Delta z} \right]^3}}, \quad (20)$$

where  $c=5$  and  $\Delta z$  is the height difference between the centres of two model layers. The asymptotic mixing length  $\lambda_h$  is taken to be 450 m. We will refer to this diffusion scheme as L6. A plot of the mixing length and asymptotic mixing length for heat in the different schemes is shown in Fig. 1.

### 2.3 $^{222}\text{Rn}$ emission

$^{222}\text{Rn}$  is emitted at a relatively uniform rate from the soil on the continents. It is relatively insoluble in water, inert and not efficiently removed by rain. It has a mean e-folding lifetime of about 5.5 days due to radioactive decay. It is assumed that the average flux from the soil lies somewhere between 0.8 and 1.3 atoms  $\text{cm}^{-2} \text{s}^{-1}$  (Liu et al., 1984; Turekian et al., 1977; Wilkening and Clements, 1975). Oceans are also a source for  $^{222}\text{Rn}$ . However, the mean oceanic flux is estimated to be 100 times weaker than the continental source (Lambert et al., 1982; Broecker et al., 1967). The fact that  $^{222}\text{Rn}$  has a lifetime and source characteristics that are similar to the lifetime and source characteristics of air pollutants

such as  $\text{NO}$ ,  $\text{NO}_2$ , propane, butane and other moderately reactive hydrocarbons, makes it interesting for evaluation of transport parameterisations.

We adopted the  $^{222}\text{Rn}$  emission scenario recommended by WCRP (Jacob et al., 1997): land emission between  $60^\circ \text{S}$  and  $60^\circ \text{N}$  is 1 atoms  $\text{cm}^{-2} \text{s}^{-1}$ ; land emission between  $70^\circ \text{S}$  and  $60^\circ \text{S}$  and between  $60^\circ \text{N}$  and  $70^\circ \text{N}$  is 0.005 atoms  $\text{cm}^{-2} \text{s}^{-1}$ ; oceanic emission between  $70^\circ \text{S}$  and  $70^\circ \text{N}$  is 0.005 atoms  $\text{cm}^{-2} \text{s}^{-1}$ . This leads to a global  $^{222}\text{Rn}$  emission of 16 kg per year. We did not account for any regional or temporal variation in the emission rate.

## 2.4 Measurements

### 2.4.1 ABL height measurements

ABL height observations from two mid-latitude sites are used in this study. They are made in Cabauw (the Netherlands) and during the FIFE campaign in Manhattan (Kansas, United States). The ABL height in Cabauw ( $52.0^\circ \text{N}$ ,  $4.9^\circ \text{E}$ ) is derived from measurements with a wind profiler during the day, and with a SODAR (Sound Doppler Acoustic Radar) during the night. The wind profiler is a pulsed Doppler radar. The strength of the echo from the radar pulse depends on the turbulence intensity. In the clear air case (no clouds or rain drops), the strength of the echo is directly proportional to the eddy dissipation velocity, and ABL heights can be derived from it in a straightforward manner. ABL heights below 2 km are measured with a resolution of 100 m and ABL heights above 2 km with a resolution of 400 m. The SODAR measures wind velocities and wind directions between 20 and 500 m by emitting sound pulses and measuring the reflection of this pulse by the atmosphere. The ABL height is available as 30-min averages. The Cabauw observations that are available to us were performed during 12 days in the summer of 1996.

The second set of ABL height measurements was made during the field experiments of the First ISLSCP Field Experiment (FIFE) (Sellers et al., 1988), which were performed

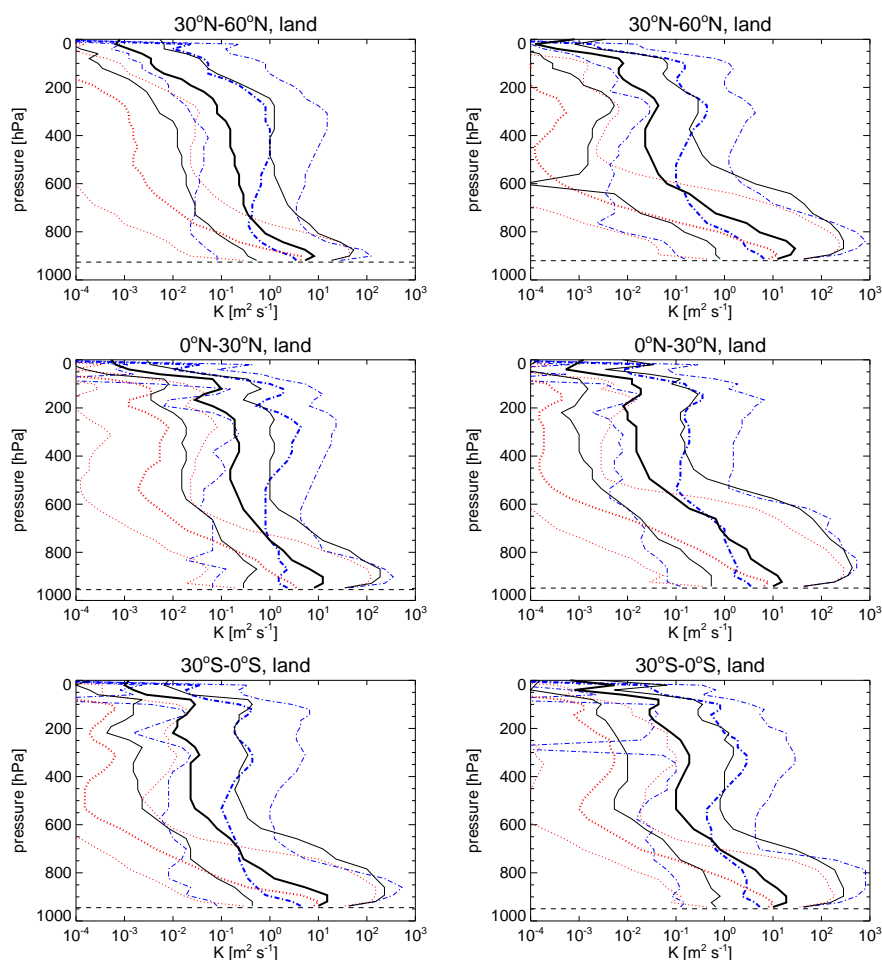


**Fig. 2.** Profiles of  $K_z$  [ $\text{m}^2/\text{s}$ ] in January (left) and July (right) 1993 over land as a function of pressure level. Profiles are given separately for 3 latitude bands. The solid black line denotes the E3/E6 case, the dotted red line the H3 case, and the dot-dashed blue line the L6 case. The thick lines denote the median, the thin lines denote the 10- and 90-percentile. The mean surface pressure level is indicated as the horizontal dashed line. For an overview of the different cases, see Table 1.

**Table 1.** Overview of the diffusion schemes.

code	scheme	time step	data origin	$K_z$	ABL height
E3	non-local	3 h	archived	averaged	
H3	non-local	3 h	off-line diagnosed	instantaneous	instantaneous
E6	non-local	6 h	archived	averaged	instantaneous
L6	local	6 h	off-line diagnosed	instantaneous	
N	no diffusion				

in 1987 and 1989 near Manhattan. Measurements of ABL height were done with a Volume Imaging LIDAR (Eloranta, 1994) and with a SODAR (Wesely, 1994). The Volume Imaging LIDAR is an elastic backscatter LIDAR that uses atmospheric light-scattering particles as tracers. It measures the radial component of the air velocity, and operates at a wavelength of 106.4 nm. Measurements are available for 22 days in the summer of 1987 and 1989. The time resolution

of the data is about 30 min. The SODAR in Manhattan (Wesely, 1994) measured during day as well as night and gave estimates of the height of the mixed layer and the vertical dimensions of inversions within the lowest kilometre of the atmosphere. It worked at a frequency of 1500 Hz. It has measured during 42 days in summer of 1987. The data is available as 30 min averages, and the vertical resolution is approximately 25 m.

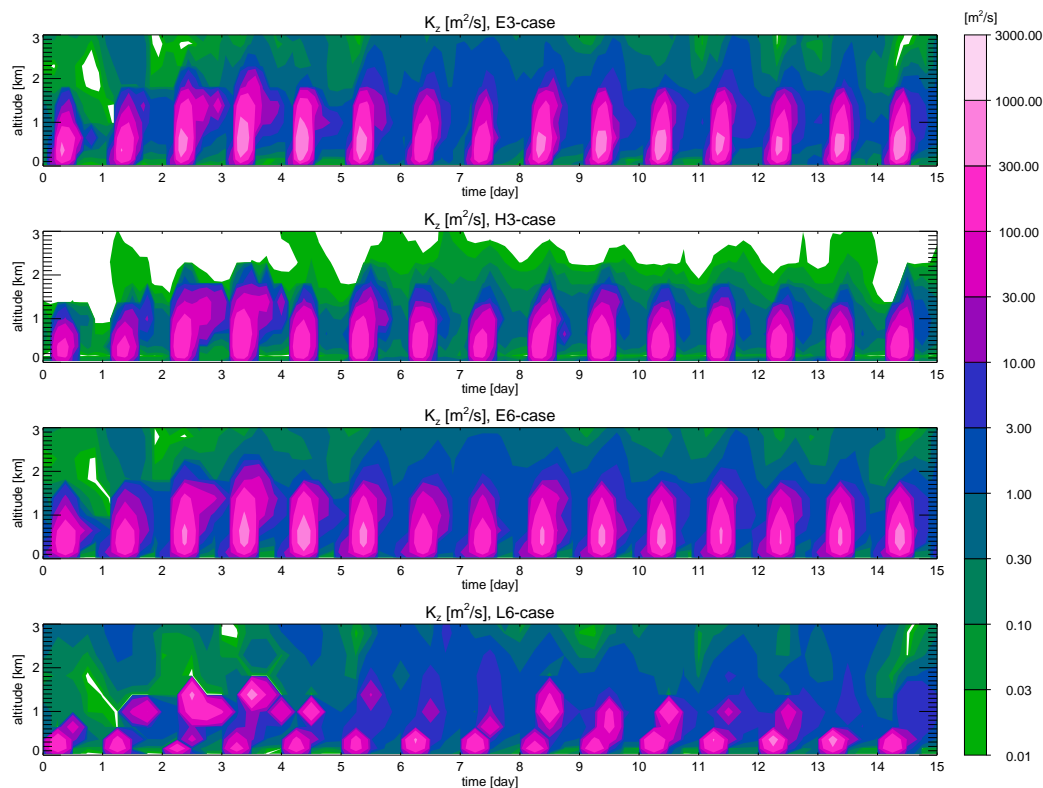


**Fig. 3.** Time series of  $K_z$  profile [ $\text{m}^2/\text{s}$ ] in lowest 3 km of the atmosphere at  $80^\circ \text{E}$  and  $20^\circ \text{N}$  (India) from 1 until 15 January 1993.

#### 2.4.2 $^{222}\text{Rn}$ measurements

$^{222}\text{Rn}$  observations from four stations are used in this study. Hourly measurements of  $^{222}\text{Rn}$  at Freiburg and Schauinsland (both at  $48^\circ \text{N}$ ,  $8^\circ \text{E}$ ) for the year 1993 are used. These data have also been used in a study by Dentener et al. (1999). Freiburg and Schauinsland are located at heights of 300 and 1200 m above sea level respectively. Schauinsland is located approximately 12 km south of Freiburg. Because the orography on horizontal scales smaller than 150 km is not resolved in the TM3 model at mid-latitudes, the observations at the Schauinsland station are not compared with the concentrations from the lowest model layer, but with the concentrations from the model layer at 900 m above the surface.

$^{222}\text{Rn}$  measurements were made in Cincinnati ( $40^\circ \text{N}$ ,  $84^\circ \text{W}$ ) at 8:00 and 15:00 LT from January 1959 until February 1963. The monthly mean  $^{222}\text{Rn}$  concentrations at these two times of the day have been taken from the literature (Gold et al., 1964). The measurements in Cincinnati were in the past extensively used in tracer transport models but never allowed a direct comparison. The ERA-40 reanalysis, which starts from the year 1957, now allows a month-to-month comparison of these measurements.

In Socorro ( $34^\circ \text{N}$ ,  $107^\circ \text{W}$ ) measurements of  $^{222}\text{Rn}$  in the atmosphere over a 6-year period have been made between

1951 and 1957. Monthly mean daily cycles over this period of the  $^{222}\text{Rn}$  concentration in Socorro ( $34^\circ \text{N}$ ,  $107^\circ \text{W}$ ) are published in Wilkening (1959). Although the measurements were not continuous (only 692 days were sampled during this period), they give a good indication of the average monthly mean daily cycle of the  $^{222}\text{Rn}$  concentration in Socorro.

#### 2.5 Experiments

We have performed model simulations with the TM3 model separately for each of the available sets of vertical diffusion coefficients. We performed 5 simulations, each with different vertical diffusion coefficients. The 5 model setups are: (E3) using 3-hourly averaged fields from the scheme in Sect. 2.2.1; (H3) using 3-hourly instantaneous fields from the first scheme in Sect. 2.2.2; (E6) as E3 but with 6-hourly averaged fields; (L6) using 6-hourly instantaneous fields according to the second scheme in Sect. 2.2.2; and (N) using no diffusion. Table 1 gives an overview of the different model simulations. The model is used with a horizontal resolution of  $2.5^\circ \times 2.5^\circ$  and 31 layers up to 10 hPa. The lowest layer has a thickness of about 60 m, the second layer of about 150 m.

For comparison with the  $^{222}\text{Rn}$  observations in Freiburg and Schauinsland, we performed model simulations from November 1992 until December 1993. November and December 1992 are included as a spin up period, and the

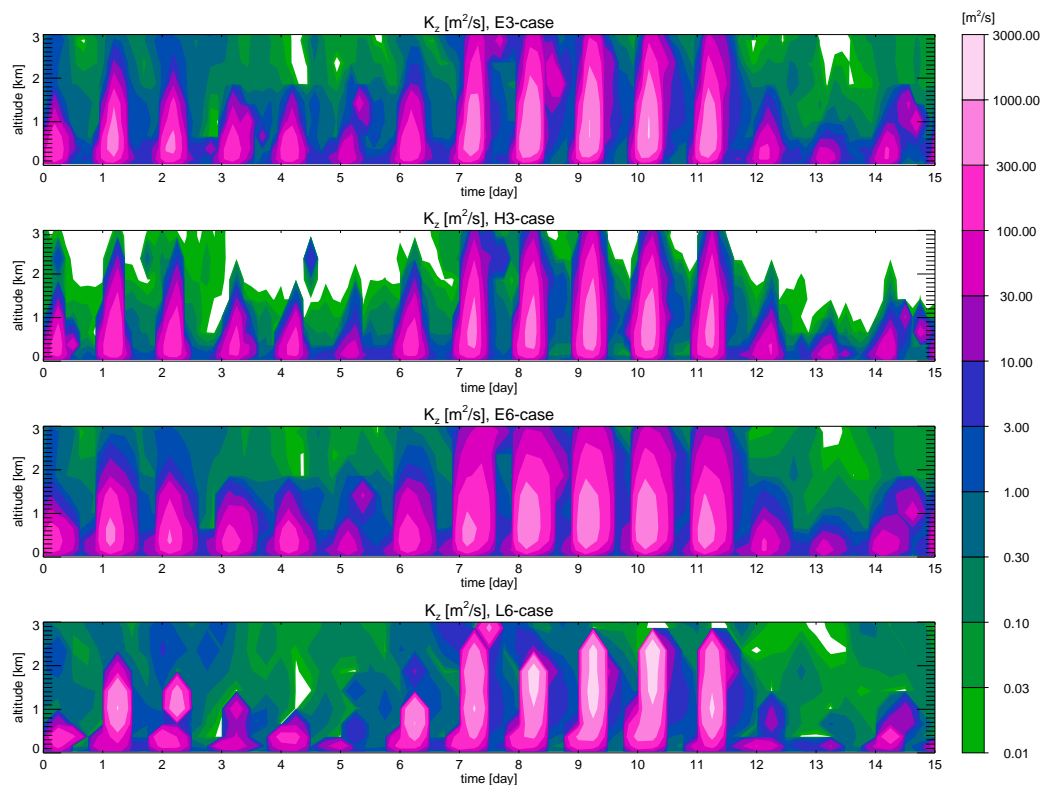


**Fig. 4.** Time series of  $K_z$  profile [ $\text{m}^2/\text{s}$ ] in lowest 3 km of the atmosphere at  $140^\circ \text{E}$  and  $20^\circ \text{S}$  (Australia) from 1 until 15 January 1993.

analysis is restricted to the year 1993. To allow comparisons with  $^{222}\text{Rn}$  measurements in Socorro and Cincinnati, we made model simulations from November 1958 until February 1963. We analyzed the period from January 1959 until February 1963 and used November and December 1958 as a spin up period. For this period we did not perform an E3-simulation.

### 3 Results

#### 3.1 Comparison of the diffusion coefficients

Zonally averaged  $K_z$  profiles from the E3/E6 scheme, the H3 scheme, and the L6 scheme are shown in Fig. 2 for January and July 1993. High values between the surface and 600 hPa correspond to the presence of an ABL, a local maximum around 300 hPa corresponds to strong vertical wind gradients in the upper troposphere. Between 900 and 600 hPa over land, the 90-percentile  $K_z$  value is almost a factor 10 smaller in winter than during summer. The largest differences between the data sets can be found above the ABL. In the free atmosphere the L6 diffusion coefficients are 2 to 3 orders of magnitude larger than the H3 diffusion coefficients. This is mainly due to the difference in the asymptotic mixing length: 450 m in the L6 case, 30 m in the H3 case. The E3/E6 co-

efficients in the free atmosphere have values between the L6 and H3 case.

We studied time series of  $K_z$  at many different sites. As an example, Figs. 3, 4 and 5 give time series of the  $K_z$  profile in the lowest 3 km of the atmosphere at 3 different locations: at  $80^\circ \text{E}$  and  $20^\circ \text{N}$  (India) in January 1993, at  $140^\circ \text{E}$  and  $20^\circ \text{S}$  (Australia) in January 1993, and at  $150^\circ \text{W}$  and  $30^\circ \text{N}$  (Pacific Ocean) in July 1993. In the ABL, the profile of  $K_z$  in the H3 case is very similar to the E3/E6 case. The vertical extent of the intense  $K_z$  values is a bit smaller than in the E3/E6 case. In the H3 case, the values are also slightly less intense, except in the winter over the continent at mid-latitudes. Also in these time series, one can observe the very low values in the free troposphere in the H3 case. There is a slightly higher variability in the E3 than in the H3 case (see Fig. 5), which might be due to the archival of  $K_z$  (E3) versus off-line diagnosis of  $K_z$  (H3): only every 6 h, new profiles of temperature, humidity and wind are used in the H3 case.

The  $K_z$  value in the L6 case differs often strongly from the other data sets. At mid-latitudes, E6 is much stronger in winter. Above sea, the vertical extent of the ABL is much smaller (see Fig. 5). Also the profile of  $K_z$  is sometimes very different, because one finds locally sometimes very high  $K_z$  values in the L6 profile: above sea (see Fig. 5), in the subtropics over land in the upper part of the ABL (see Fig. 4),

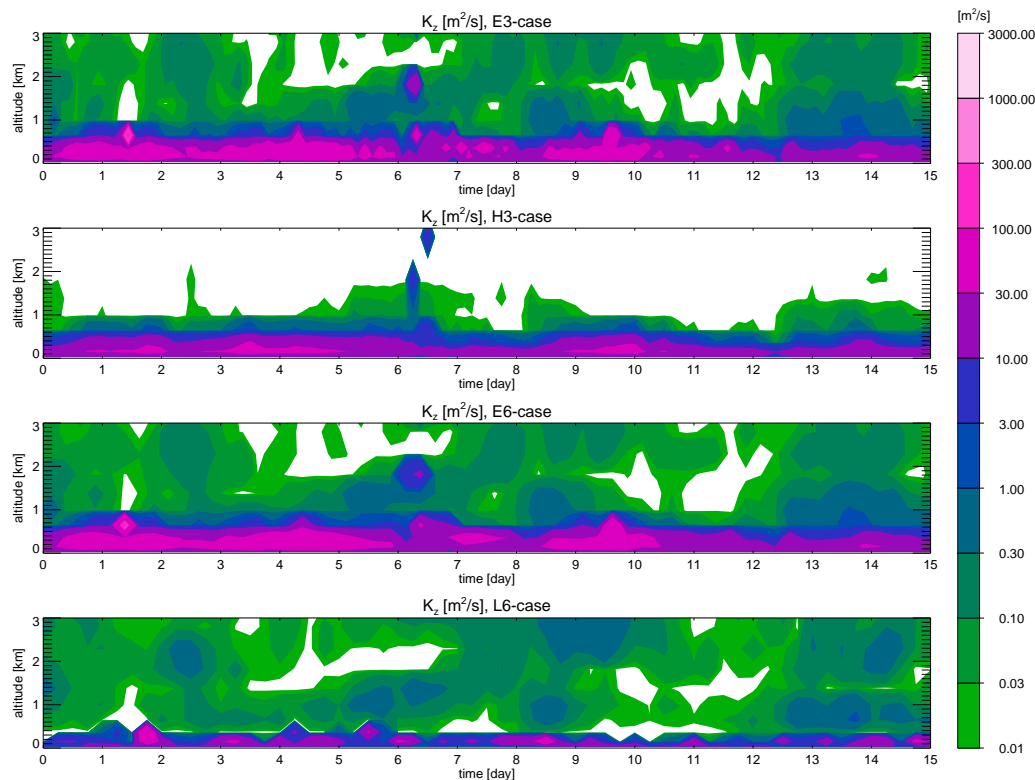


**Fig. 5.** Time series of  $K_z$  profile [ $\text{m}^2/\text{s}$ ] in lowest 3 km of the atmosphere at  $150^\circ \text{W}$  and  $30^\circ \text{N}$  (Pacific Ocean) from 1 until 15 July 1993.

or as disconnected spots in Fig. 3. Although the strong deviation for the L6 case which is caused by the local nature of the scheme, there is still a strong similarity with the other  $K_z$  profiles. This is due to the fact that the L6  $K_z$  values are based on atmospheric profiles of temperature, humidity and wind, which carry the imprint of the ABL scheme used during ERA-40.

### 3.2 Evaluation of the model simulated atmospheric boundary layer height

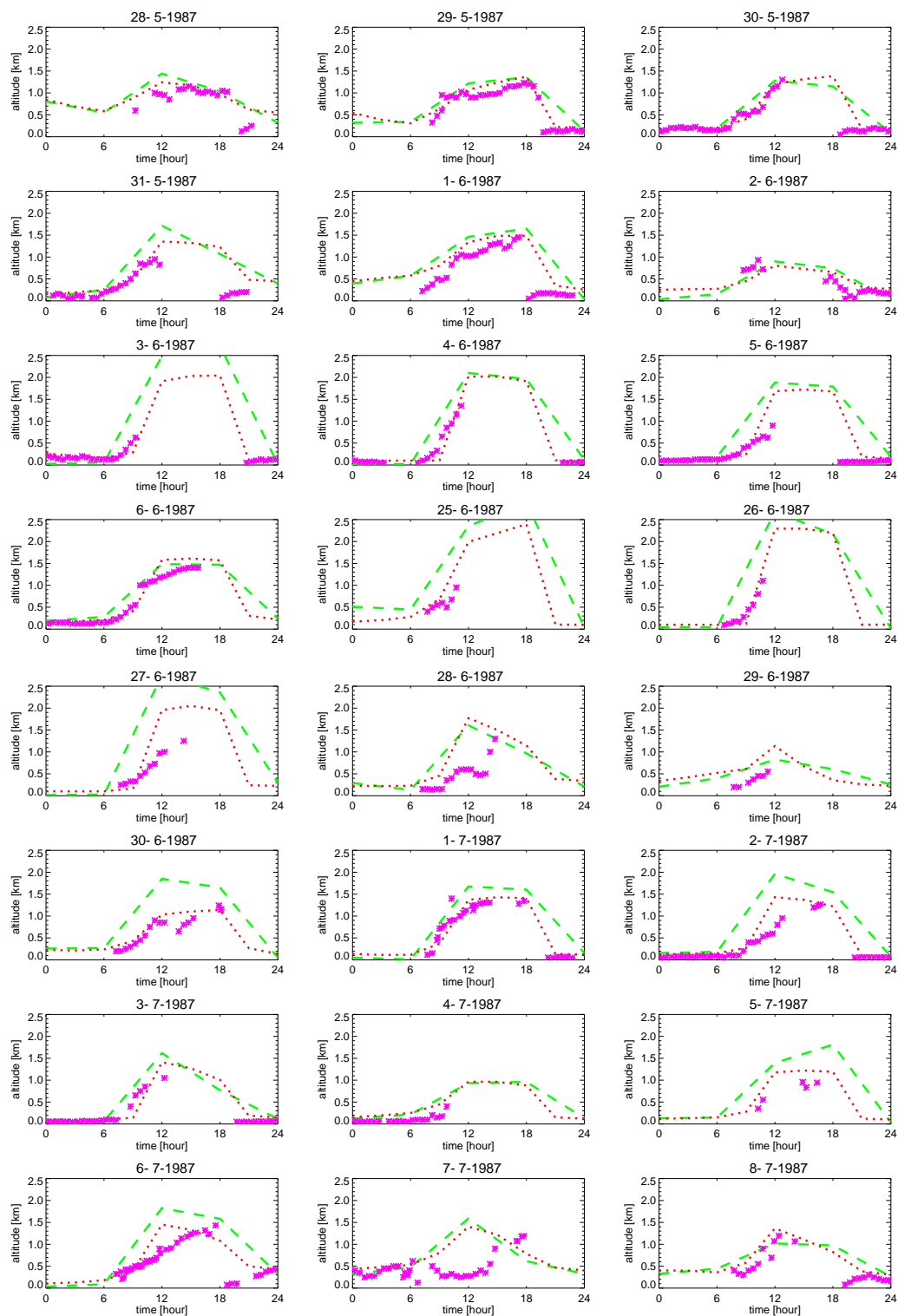
We compared the 6-hourly ABL height from the ERA-40 data (E6), and the 3-hourly ABL height diagnosed in the H3-scheme with ABL heights observed in Cabauw and during the FIFE campaign. The calculated and measured ABL heights during the FIFE campaign are shown in Fig. 6 (only a subset of the data is shown); for Cabauw they are shown in Fig. 7 (all data is shown). The maximum value of the height of the ABL is quite well represented both for the E6 and H3 case. Also the time of strongest growth and decrease is well represented.

Figure 8 gives a scatter plots of the measured ABL height during the FIFE campaign versus the modelled ABL height for the cases E6 and H3 separately. A distinction is made between measurements made during daytime and measurements made during nighttime. At the end of the day (obser-

vations before 21:00 LT) we see that the observations and measurements do not correspond very well (the model ABL height is much larger). At this time of the day, the ABL is hard to define anyway: a stable inversion layer is building up below the residual layer. Later during the night we see that the agreement between the observations and model is much better. It is clearly visible in Fig. 8 that the ABL height with low as well as with high wind speeds corresponds well between model and observations. The H3 case gives a better agreement than the L6 case.

Also during daytime there is a good agreement. For both cases (E6 and H3), the modelled ABL height is larger than observed: the H3 ABL height corresponds however slightly better with the observations. The higher ABL height in the E6 case can be caused by the smaller coefficient for the excess of the parcel temperature under unstable conditions. It also shows that a 6-hourly resolution is rather coarse for describing the ABL height evolution.

Due to the limited amount of data in Cabauw, we only look at the time evolution of the ABL height in Fig. 7. We see that the quality of the ERA-40 ABL height and the H3 ABL height are similar: for both schemes, the ABL height in the afternoon falls off in the model sometimes too fast, and is at night sometimes too high. Comparison of the ABL height between model and observations is hampered by representation



**Fig. 6.** Time evolution of the ABL height during the FIFE campaign in 1987 and 1989 in the US. Pink stars denote the observed ABL height, the dashed green line denotes the ABL height archived in the ERA-40 data (E6), the dotted red line denotes the ABL height calculated in the H3-scheme. The time is expressed in GMT+6h.

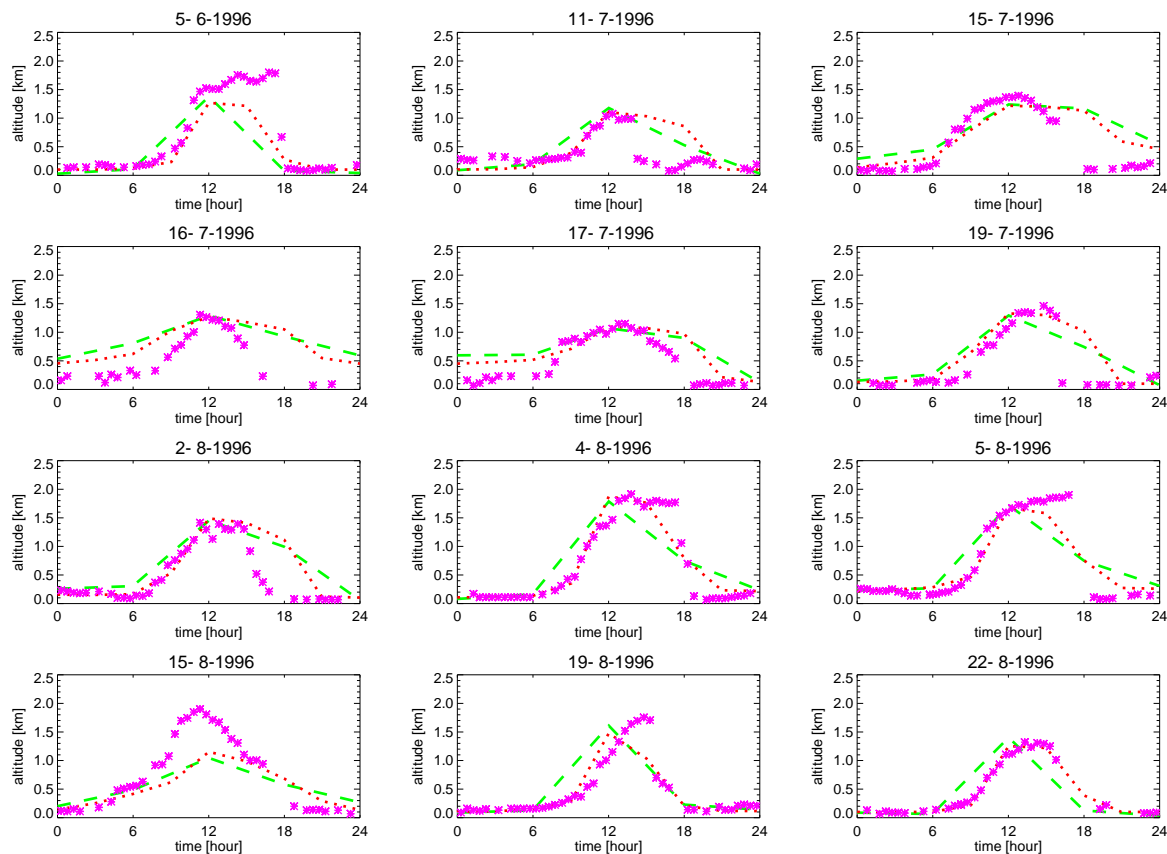


**Fig. 7.** Time evolution of the ABL height during some days in June, July and August 1996 in Cabauw, the Netherlands. Symbol and line code as in Fig. 6. The time is expressed in GMT.

errors in modelled fluxes, the presence of clouds during day-time, and limited space and time resolution of the model. Bosveld et al. (1999) have compared observed heat fluxes with modelled heat fluxes from ERA-15 at Cabauw. They found that the ECMWF model underestimates the amount of clouds at Cabauw, which leads to excessive surface heating, resulting in too large surface heat fluxes. Similar deficiencies seem to be present in the ERA-40 data.

Despite the rather limited comparison with measurements, we can conclude that the ABL heights as calculated during the ERA-40 project (E6) and with the H3 scheme, agree reasonably with the measurements during summer in mid-latitudes.

### 3.3 Comparison with $^{222}\text{Rn}$ measurements in Freiburg and Schauinsland

We compared the simulated  $^{222}\text{Rn}$  concentrations from the TM3 model with surface observations from Freiburg and Schauinsland. Time series of modelled and observed  $^{222}\text{Rn}$  concentrations are shown in Fig. 9 for the first 15 days of June and September 1993.

**Table 2.** Mean value of the  $^{222}\text{Rn}$  concentration [ $10^{-21}$  mol/mol] in 1993 in Freiburg and Schauinsland.

diffusion	Freiburg	Schauinsland
E3	102±45	33±15
H3	110±59	33±16
E6	98±41	34±15
L6	125±68	32±16
N	501±113	26±17
observed	113±70	37±19

#### 3.3.1 Seasonal cycle of the modelled and measured $^{222}\text{Rn}$ concentration

The monthly mean values of the  $^{222}\text{Rn}$  concentration, the correlation of the modelled with the observed daily mean values, and the correlation of the residues for the year 1993 in Freiburg and Schauinsland are shown in Fig. 10 (the residue is defined as the hourly concentration minus the daily mean concentration). Table 2 gives the 1993 yearly mean  $^{222}\text{Rn}$

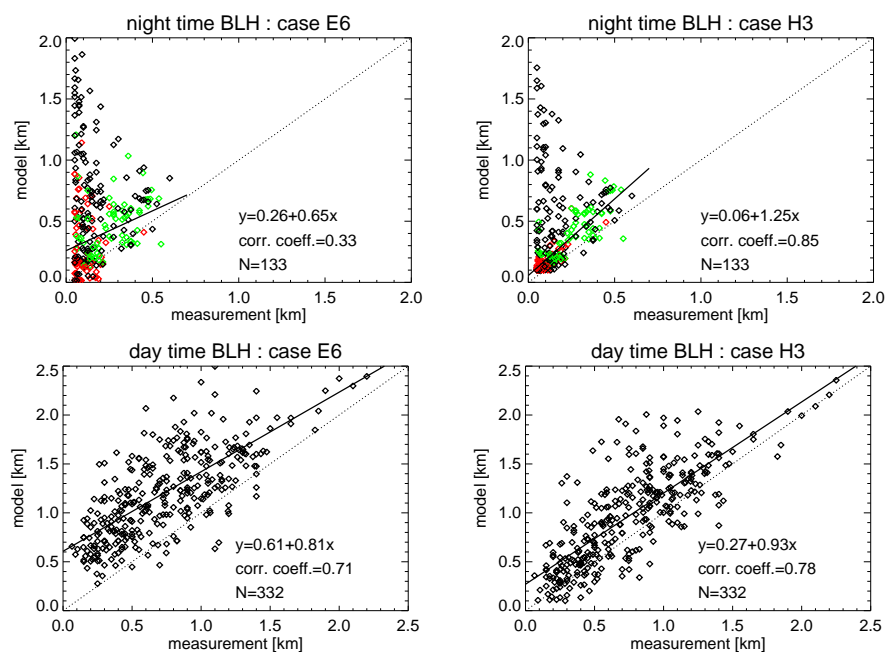


**Fig. 8.** Scatter plot of the measured ABL height during the FIFE campaign versus the modelled ABL height for E6 (left) and H3 (right). In the upper panel the nighttime observations are shown: black signs refer to measurements before 21:00 LT, green signs (wind speed >3 m/s) and red signs (wind speed <3 m/s) refer to measurements after 21:00 LT. The regression line for the nighttime is only based on the observations after 21:00 LT. In the lower panel the daytime observations are shown.

**Table 3.** Correlation of the modelled with the observed  $^{222}\text{Rn}$  concentration in 1993 in Freiburg and Schauinsland. In column (a) the correlation of the modelled with the observed daily mean is given, in column (b) the correlation of the modelled with the observed hourly value, and in column (c) the correlation of the modelled with the observed residue (the residue is defined as the hourly concentration minus the daily mean concentration).

diffusion	Freiburg			Schauinsland		
	(a) (N=306)	(b) (N=7731)	(c) (N=7344)	(a) (N=243)	(b) (N=7250)	(c) (N=5832)
E3	0.870	0.773	0.498	0.589	0.508	0.282
H3	0.871	0.790	0.522	0.528	0.455	0.242
E6	0.871	0.759	0.449	0.596	0.509	0.262
L6	0.844	0.735	0.484	0.538	0.477	0.286
N	0.704	0.648	0.364	0.400	0.347	0.125

concentration. All schemes reproduce the monthly mean values quite well, both in Freiburg and in Schauinsland. In Freiburg, the spread in mean concentration between the different diffusion schemes is about 20%. The L6 scheme results in the highest mean concentrations, the E6 scheme in the lowest mean concentrations. The E3 case gives almost similar results as the E6 scheme. In Schauinsland, the spread in the modelled result is much smaller (except in February), but the agreement with the measurements is smaller. For both stations, the correlation of the modelled with the observed mean daily value is higher than the correlation of the modelled with the observed hourly value (not shown), and

the correlation of the modelled with the observed residue is smallest. It clearly shows that the variation of the  $^{222}\text{Rn}$  concentration by large scale synoptic variability is well modelled, and that the variation of the  $^{222}\text{Rn}$  concentration due to local and short time scale phenomena (like diffusion) is harder to describe. There is also a remarkable difference between the correlation of the modelled with the observed residue between the E6 and the E3 case, as well in Freiburg as Schauinsland. Table 3 gives the correlations between the observed and modelled  $^{222}\text{Rn}$  concentration during 1993.

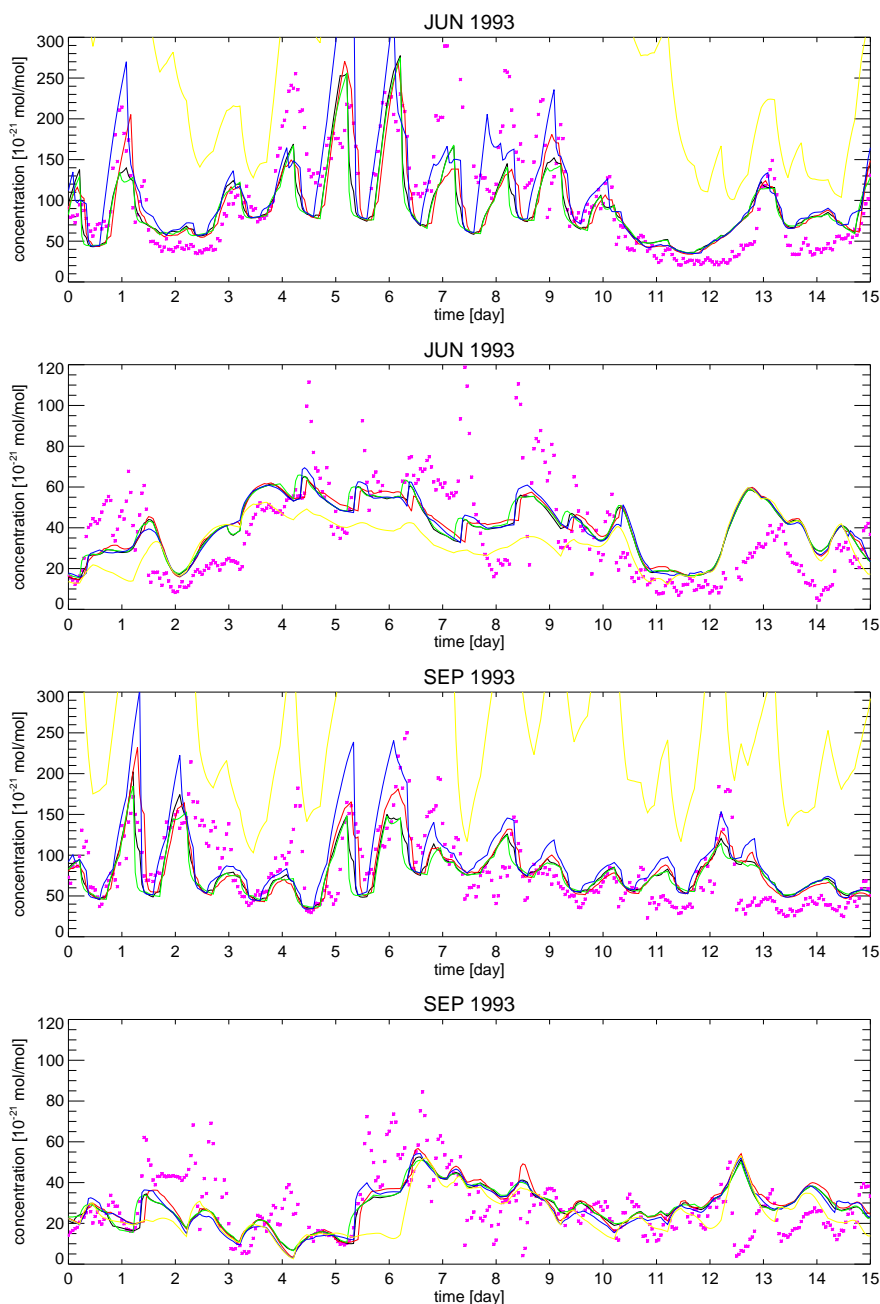


**Fig. 9.** Time series of  $^{222}\text{Rn}$  concentration [ $10^{-21}$  mol/mol] in first 15 days of June and September 1993 for Freiburg (1st and 3rd panel) and Schauinsland (2nd and 4th panel). The pink stars denote the observations, the lines denote the results from the model runs: using E3 data (black line), using H3 data (red line), using E6 data (green line), using L6 data (blue line), and using no diffusion (yellow line).

### 3.3.2 Daily cycle

The mean daily cycle of the  $^{222}\text{Rn}$  concentration in Freiburg and Schauinsland for December, January and February (DJF) and for June, July and August (JJA) are shown in Fig. 11. In Freiburg, the daily cycle of the L6 case is largest. The E3 and E6 cases are very similar, except for the periods 6:00–9:00 and 15:00–21:00 (only in DJF) where the E6 case results in

lower  $^{222}\text{Rn}$  values. For all schemes the daytime concentrations are almost the same in JJA, while differences persist in DJF.

The daily cycle in the model simulations in Schauinsland is clearly not as strong as in the measurements. The deviation is quite large in DJF. In JJA, the simulations reproduce an increase in the concentration in the morning, but not large enough. The schemes differ in the time positioning

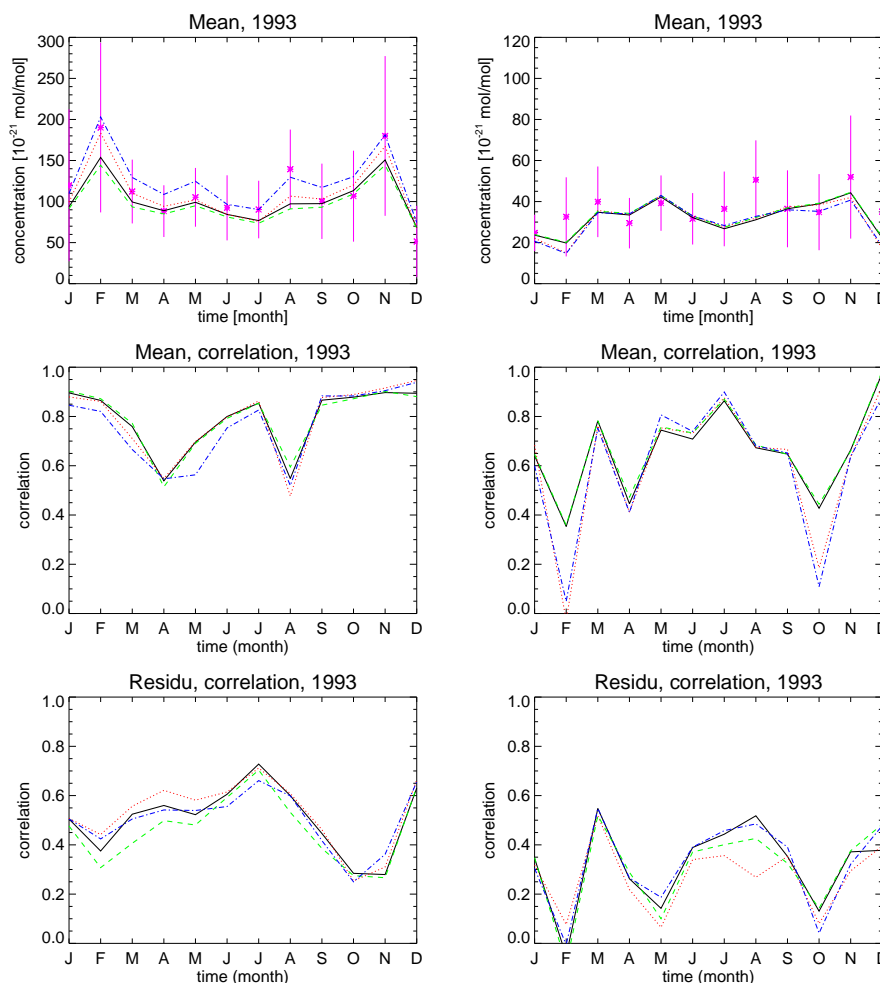


**Fig. 10.** Monthly mean  $^{222}\text{Rn}$  concentration (upper panels), correlation of the modelled with the observed mean daily value (middle panels), and correlation of the observed with the modelled deviation (lower panels), for Freiburg (left) and Schauinsland (right) in 1993. The pink stars denote the mean observations, the lines denote the results from the model runs: using E3 data (solid black line), using H3 data (dotted red line), using E6 data (dashed green line), and using L6 data (dot-dashed blue line). The error bars (upper panels) show the  $1\sigma$  standard deviation of the observations.

of this increase. The second maximum in the measurements in JJA in Schauinsland is clearly not present in the model simulations (except for the H3 case). In Fig. 11, one can clearly identify the times when the meteorological fields are updated.

The daily minimum, daily maximum and daily amplitude of the  $^{222}\text{Rn}$  concentration are closely related to the daily cycle of the ABL turbulence. In Fig. 12 the monthly mean value of the daily minimum, maximum and amplitude are shown. It can be seen that in Freiburg these values correspond quite well with the measurements. The amplitude is slightly overestimated by the L6 scheme, while it is underestimated by the E3, H3 and E6 scheme. At the same time the correlation (not shown) of the modelled with the observed daily amplitude is considerably smaller than the correlation of the modelled with the observed daily minimum or daily

maximum. In Schauinsland, we see that the minimum values in the model are in general higher than the observed minimum values, that the maximum values are in general smaller than the observed values, and that the modelled amplitude is therefore much smaller than the observed amplitude. The amplitude in the L6 case is largest. In Schauinsland, the variation between the schemes is much smaller than in Freiburg. All this shows that the coarse time and spatial resolution of the model limit its ability to reproduce variations on short time scales.

### 3.3.3 Ratio between $^{222}\text{Rn}$ concentration in Freiburg and Schauinsland

Because the stations at Freiburg and Schauinsland are close to each other (12 km), and the station at Schauinsland lies

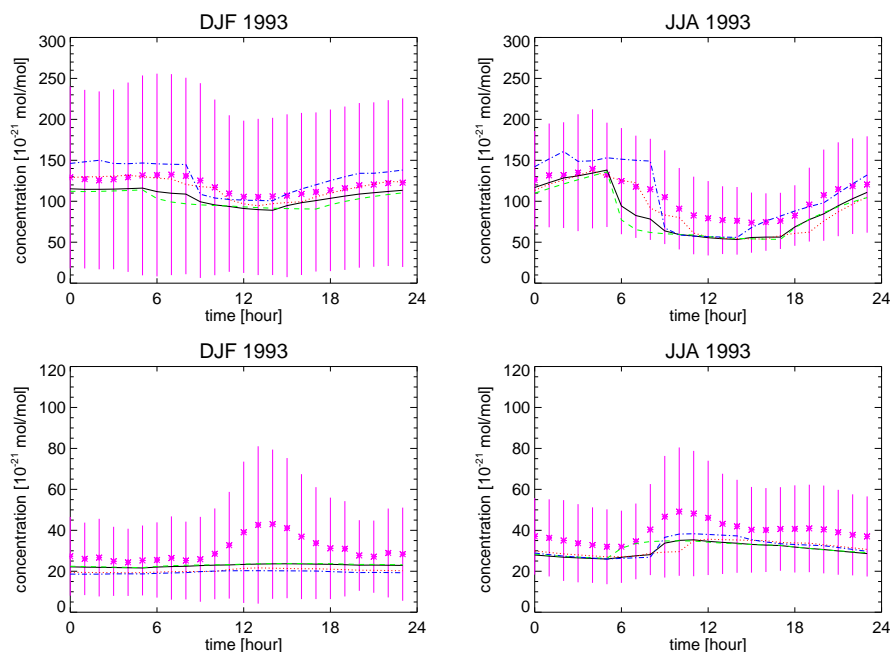


**Fig. 11.** Daily cycle of observed and modelled  $^{222}\text{Rn}$  concentration in Freiburg in DJF (upper left) and JJA (upper right) and in Schauinsland in DJF (lower left) and JJA (lower right) 1993. The stars denote the observed value, the lines denote the modelled values (line code is as in Fig. 10). The error bars show the  $1\sigma$  standard deviation of the observations.

on a hill 900 m higher than Freiburg, these stations are quite well suited to study vertical concentration gradients in the model. Ideally we would prefer to use co-located observations, however tower measurements were not available to us.

The ratio of the  $^{222}\text{Rn}$  concentration in Freiburg (300 m above sea level) and Schauinsland (1200 m above sea level) is assumed to be less sensitive to errors in the  $^{222}\text{Rn}$  emission and to influences of large-scale transport (synoptic variability). In Fig. 13 and Table 4 the correlation between the ratio in the model and the ratio in the measurements is given. This value of the correlation lies close to the correlation of the hourly value in Freiburg, and is significantly higher than the correlation of the hourly concentration in Schauinsland (see Table 3).

Because we expect a strong dependence of the aforementioned ratio on the ABL height, we have grouped the measured and modelled ratios as a function of the height of the ABL. For the height of the ABL we took the values of the ABL height as they are calculated in the H3 scheme: they are calculated every 3 h and correspond well with observations (see Sect. 3.2). Because the  $^{222}\text{Rn}$  data are available hourly, we interpolated the ABL height to an hourly resolution. (We also tried this with the 6-hourly ABL heights from the ERA-40 data set. We noticed however that this gave more noisy relationships due to the coarser time resolution of the E6 ABL height.)

In Fig. 13 one can observe that the ratio becomes smaller as a function of the height of the ABL. We would expect

**Table 4.** Correlation between the observed and modelled ratio of the  $^{222}\text{Rn}$  concentration in Freiburg and in Schauinsland in 1993.

diffusion	Freiburg/Schauinsland (N=6531)
E3	0.758
H3	0.772
E6	0.741
L6	0.717
N	0.575

the ratio to go to one when the ABL height reaches higher than the station in Schauinsland: one expects hyperbolic behaviour for ABL heights below 800–1000 m, and a sharp drop in the ratio around 800–1000 m. We see however that as well for the observed ratio as for the modelled ratio, the transition point is around 500 m, and not around 800–1000 m. This can be related to the coarse vertical resolution between 500 and 1000 m, the large scatter of the data, and the use of a modelled ABL height to deduce these curves. The E3/E6 scheme shows the strongest correspondence with the measurement, the H3 and L6 scheme show the worst correspondence. Also from this graph it is clear that the E3 and E6 case cause stronger mixing than the H3 and L6 case. In general this Fig. 13 shows that, despite of the failure of the scheme's to reproduce all the short time scale variations, the mean variations in the ratio are reasonably captured.

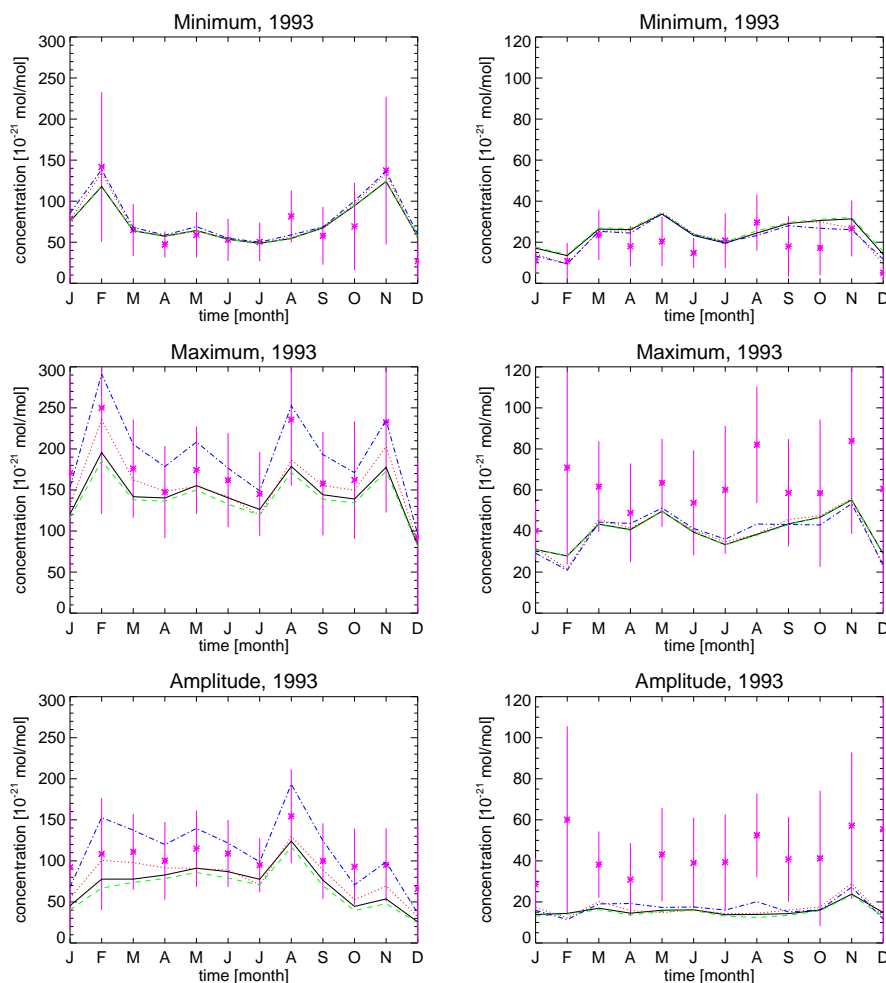


**Fig. 12.** Monthly mean of the daily minimum (upper panels), daily maximum (middle panels) and daily amplitude (lower panels) in the  $^{222}\text{Rn}$  concentration in Freiburg (left) and Schauinsland (right) in 1993. The stars denote the measurements, the lines denote the results from the model runs (line code as in Fig. 10). The error bars show the  $1\sigma$  standard deviation of the observations.

**Table 5.** Correlation of the observed with the modelled  $^{222}\text{Rn}$  concentration in Cincinnati and Socorro.

diffusion	Cincinnati		Socorro
	morning (N=48)	afternoon (N=48)	daily cycle (N=288)
H3	0.523	0.388	0.823
E6	0.639	0.399	0.714
L6	0.711	0.421	0.759

### 3.3.4 Time shift

The diffusive and convective mass fluxes are updated in the TM3 model every 3 or 6 h. The updates have a strong influence on the modelled  $^{222}\text{Rn}$  distribution (see Fig. 11). The simulations show that the more frequent the updates are, the

better the correspondence with the measurements is: E3 performs better than E6, H3 performs better than L6.

Averaging of diffusion coefficients over a certain time interval leads to a strong influence of the large diffusion coefficients during a part of this interval on the time-averaged diffusion coefficient, and thus on the concentration and transport in the tracer transport model. If one compares the E6 and E3 case, it shows up as an earlier start and a sustained prolongation of the low daytime  $^{222}\text{Rn}$  values in Freiburg (see again Fig. 11). Using instantaneous diffusion coefficients can maximally lead to a time shift of half the time step, while using a time-averaged value can lead in the extreme case to a time shift of almost the whole time step. This has a considerable influence in case of time steps of 6 h. This might also play an important role for other tracers than  $^{222}\text{Rn}$  where chemistry and dry deposition come into play.

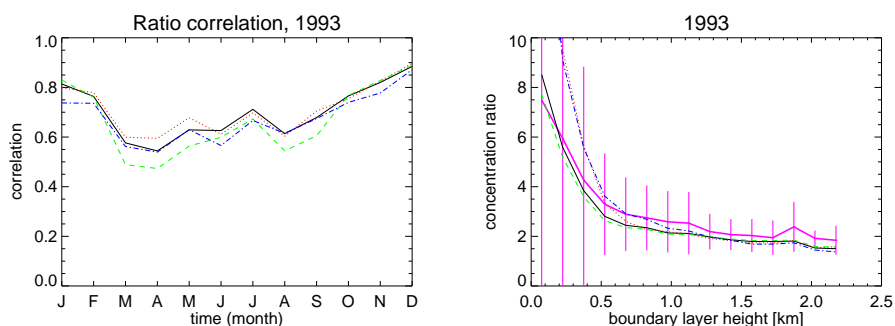


**Fig. 13.** Left panel: correlation of the modelled with the observed ratio of the concentration in Freiburg and the concentration in Schauinsland. Right panel: mean ratio between the  $^{222}\text{Rn}$  concentration in Freiburg and the concentration in Schauinsland as a function of the ABL height (calculated with the H3 scheme) for the year 1993. The thick pink line denotes the ratio derived from the observed concentrations, the other lines denote the ratio's derived from the modelled concentrations using E3 data (solid black line), using H3 data (dotted red line), using E6 data (dashed green line), and using L6 data (dot-dashed blue line). To calculate these curves, we binned all the hourly ABL height data in 15 bins with a width of 150 m, ranging from 0 up to 2250 m. The ABL height is taken from the H3 scheme. The error bars denote the  $1\sigma$  standard deviation of the ratio derived from the observed concentrations.

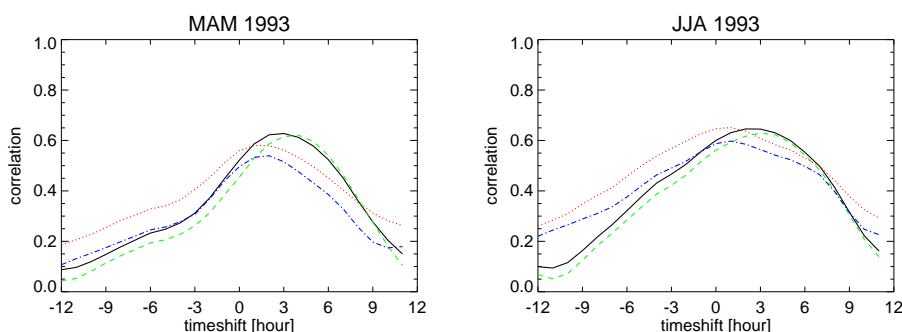


**Fig. 14.** The correlation of the hourly modelled with the hourly observed  $^{222}\text{Rn}$  concentration in Freiburg in MAM (left) and JJA (right) as a function of the time shift. Only the modelled concentration between 0:00 and 12:00 GMT is used. Values in the right hand part of the figure (positive time shifts) give the correlation of model concentrations with a later observation, values in the left part of the figure (negative time shifts) give the correlation of model concentrations with an earlier observation. Line code: using E3 data (solid black line), using H3 data (dotted red line), using E6 data (dashed green line), and using L6 data (dot-dashed blue line).

We have investigated this effect by correlating the modelled morning concentrations (from 0:00 until 12:00 GMT) with time-shifted observed concentrations. The correlation as a function of the applied time shift is shown in Fig. 14 for the periods March–April–May (MAM) and JJA. The strongest time shift is found for the E6 and E3 case (E6 stronger than E3), which both use time-averaged diffusion coefficients. The time shift is smallest for the L6 and H3 case (instantaneous values). With an applied time shift for the morning concentrations of 3 h for the E3 case, and up to 4 or 5 h in the E6 case, the E3 and E6 case perform equally good (JJA) or better (MAM) than the H3 scheme. We have also correlated the modelled afternoon concentrations (from 12:00 until 24:00) with time-shifted observed concentrations. This resulted in slightly smaller time shifts with the highest correlation for shifts back in time in the E6 and E3 case (corresponding to persistent low  $^{222}\text{Rn}$  concentrations at the end

of the day). Due to the opposite sign of the shifts between morning and afternoon, and due to a probable geographical dependence of this shift, it is not easy to implement a remedy. It shows the necessity of high sampling frequency of data.

#### 3.4 Comparison with $^{222}\text{Rn}$ measurements in Cincinnati and Socorro

Figure 15 gives the observed and modelled monthly mean surface concentration in Cincinnati for 8:00 and 15:00 LT from January 1959 until February 1963. The seasonal variation in the observations is much larger than in the model. Gold et al. (1964) attribute this to freezing minimizing the emission in winter, and to an increasing emanation rate of  $^{222}\text{Rn}$  due to the decrease of the moisture content of the soil with increase of temperature in summer. This dependence

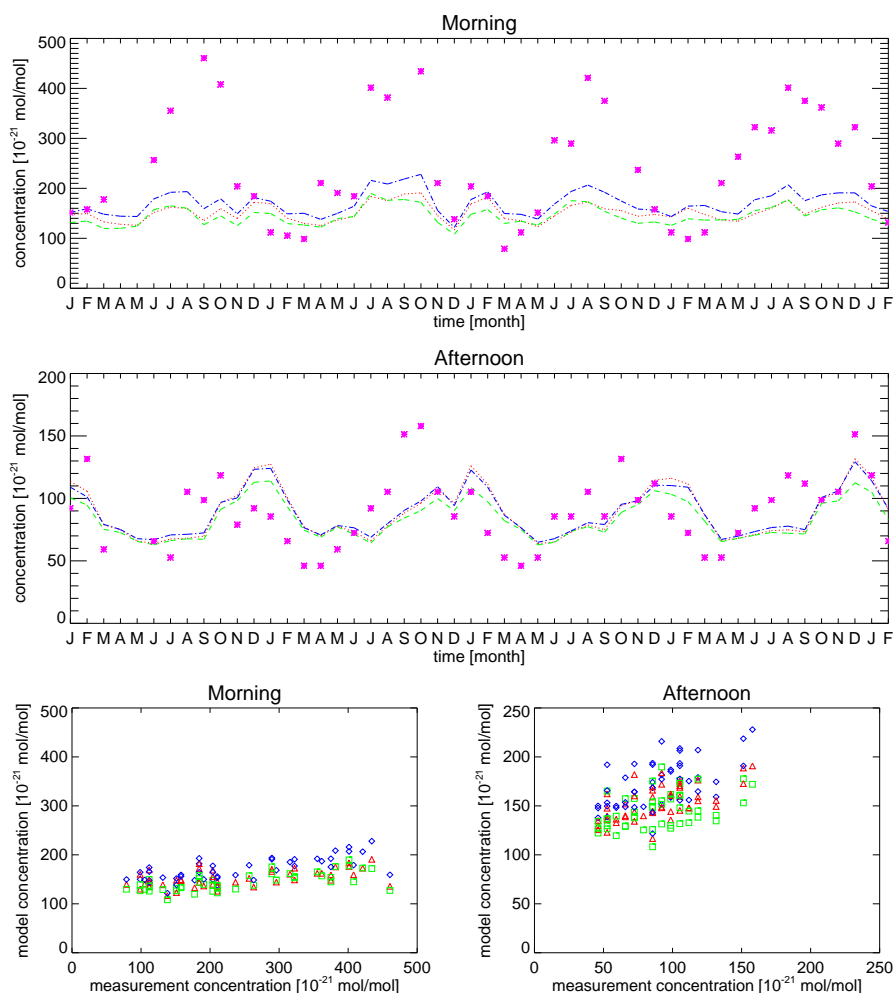


**Fig. 15.** Monthly mean morning (upper panel) and afternoon (middle panel)  $^{222}\text{Rn}$  concentration from January 1959 until February 1963 at Cincinnati. Observed concentrations (pink stars) and modelled concentrations using H3 data (dotted red line), E6 data (dashed green line), and L6 (dot-dashed blue line) are shown. Scatter plots of the monthly mean morning (lower left) and afternoon (lower right)  $^{222}\text{Rn}$  concentration are shown using H3 data (red triangles), using E6 data (green squares), and using L6 data (blue diamonds).

of the emanation of  $^{222}\text{Rn}$  on meteorological conditions is not included in the TM3 model. The poor correspondence of the morning data is probably also caused by a bad representation of the night and morning  $^{222}\text{Rn}$  profiles in the global model due to the large thickness of the lowest model layer (about 60 m), resulting in lower modelled  $^{222}\text{Rn}$  concentrations under very stable meteorological conditions. Another main reason for discrepancy is that the morning measurements represent more local conditions, which may not fulfil the  $1 \text{ atom cm}^{-2} \text{ s}^{-1}$  emission rate. Although the observed morning concentration is quite different from the modelled morning concentration, the afternoon concentrations agree quite well with the observations (see Fig. 15). As for the  $^{222}\text{Rn}$  concentrations in Freiburg, we see that the L6 scheme leads to the highest morning concentrations, while the E6 case gives the lowest values. The H3 case gives intermediate values.

Measurements of  $^{222}\text{Rn}$  have been made at Socorro from November 1951 until June 1957. These data were used to generate monthly mean daily cycles of the  $^{222}\text{Rn}$  concentration (Wilkening, 1959). We have compared the monthly mean daily cycles from January 1959 until February 1963 with these data. The result can be seen in Fig. 16. The afternoon values for E6, L6 and H3 are very similar. The mean values are given in Table 6.

### 3.5 Global $^{222}\text{Rn}$ distribution

In order to see the effect of diffusive transport on the free troposphere concentrations of tracers, we now consider the budgets and transport of  $^{222}\text{Rn}$ . Diffusion leads in general to differences of up to 30% in the zonal mean  $^{222}\text{Rn}$  concentration compared to the case where no diffusion is applied in the TM3 model. Smaller diffusion coefficients

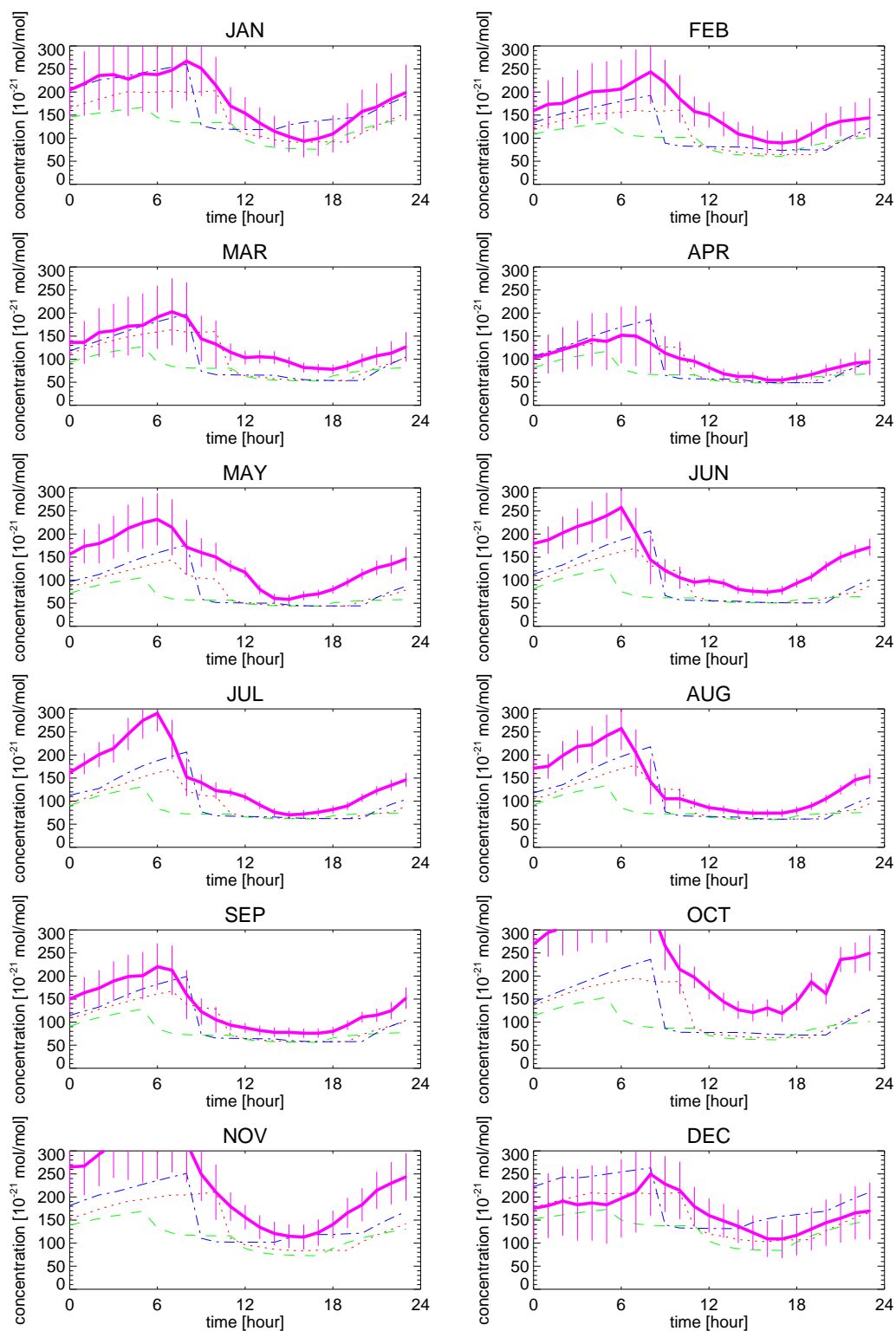


**Fig. 16.** Monthly mean daily cycle of  $^{222}\text{Rn}$  concentration from January 1959 until February 1963 in Socorro: measured (thick solid pink line) and modelled using H3 (dotted red line), using E6 (dashed green line) and using L6 (dot-dashed blue line). The observed monthly mean daily cycles are based on measurements from November 1951 until June 1957. The error bars denote the  $1\sigma$  standard deviation of the modelled concentration.

**Table 6.** Mean observed and modelled  $^{222}\text{Rn}$  concentration [ $10^{-21}$  mol/mol] at Socorro. The observations have been made between November 1951 and June 1957. The modelled concentrations are mean values for the period January 1959 until December 1962.

diffusion	Socorro
H3	113±44
E6	91±44
L6	121±44
observed	158

lead to higher  $^{222}\text{Rn}$  concentration in the lowest layers and higher concentrations higher up in the atmosphere. The influence of diffusion is strongest in the parts of the atmosphere with strong downward large-scale motion like the subtropics, and/or where there is no vertical mixing by convection. In Fig. 17, the relative difference in the zonal mean  $^{222}\text{Rn}$  concentration between the E3 and H3 case and between the E3 and L6 case is shown for DJF 1993.

In Fig. 18, the relative difference in  $^{222}\text{Rn}$  concentrations at 700 hPa between the E3 and H3 case and between the E3 and L6 case is shown for JJA 1993.

If we compare the E6 and E3 case, the zonal mean differences are everywhere smaller than 1% (not shown).

If we compare H3 and L6 with E3, we always see that the  $^{222}\text{Rn}$  concentration in the lowest 500–1000 m is lower for E3, while above 1 km it is higher for E3. This higher concentration for H3 and L6 in the lowest layers of the atmosphere, leads to higher  $^{222}\text{Rn}$  concentrations in the upper troposphere by convection, which transports the surface air to high altitudes in the tropics. We see in JJA around the North Pole higher concentrations in the lowest kilometre in the E3 case. Because there is almost no  $^{222}\text{Rn}$  emission north of  $60^\circ\text{N}$ , the concentration is higher in the free troposphere than at the surface (via long range transport). The increased mixing in the E3 case will then transport this  $^{222}\text{Rn}$  downward.

If we compare the H3 and E3 case, we see much higher concentrations in the E3 case in almost the whole troposphere (except the lowest layers). The stronger diffusion gives more mixing. Large differences can be found around 700 hPa in the winter subtropics, i.e. around  $20^\circ\text{N}$  in DJF and around  $20^\circ\text{S}$  in JJA.

If we compare L6 and E3, we see the effect of stronger diffusion in the free troposphere in the winter subtropics for L6. Through more intense and higher mixing, the  $^{222}\text{Rn}$  concentrations are 5 to 10% higher around 500 hPa and 15% lower around 800 hPa in DJF around  $20^\circ\text{N}$  and in JJA around  $20^\circ\text{S}$ .

Because  $^{222}\text{Rn}$  has a short lifetime (about 5.5 days), we can deduce the global mean net vertical  $^{222}\text{Rn}$  transport and changes therein due to differences in the diffusion schemes from its mean distribution. The net flux profile of  $^{222}\text{Rn}$  is an indication of how the vertical diffusion will affect other

tracers. This flux strongly depends on the source characteristics of the tracer (which are uniform on the continent for  $^{222}\text{Rn}$ ), and it is also strongly dependent on the sinks and the lifetime. In Fig. 19, we show the net global vertical  $^{222}\text{Rn}$  fluxes. All fluxes are expressed relative to the E3 case. The differences in net global transport are maximally 4%. The difference is largest around 900 hPa. The difference between E3 and E6 are less than 1%. The net transport for the H3 case is stronger than the E3 case above 500 hPa, and stronger for the L6 case than the E3 case above 700 hPa. The interaction between the convection and the ABL turbulence is clearly visible. One can observe the following pattern: weaker transport in the lower troposphere leads to stronger transport in and into the upper troposphere. As mentioned before, if the turbulent transport is weaker, more  $^{222}\text{Rn}$  remains in the lowest atmospheric levels, which can then be transported to the upper troposphere via fast convective transport. Higher concentrations at the surface (due to less turbulent transport) thus lead to higher concentrations in the upper troposphere.

In general, one can see in Fig. 19 that the differences in concentration and transport are quite small. This can partly be attributed to the fact that diffusion is not the only way of vertical transport. If the diffusive transport changes, it will be partly compensated by convective or large-scale vertical transport.

#### 4 Conclusions

We have studied the application of archived and off-line diagnosed vertical diffusion coefficient from the ERA-40 project for making simulations with chemistry transport models. We compared 4 sets of vertical diffusion coefficients: (E3) 3-hourly archived coefficients based on a non-local scheme, (H3) 3-hourly off-line diagnosed coefficients based on a non-local scheme, (E6) as E3 but 6-hourly values, and (L6) 6-hourly off-line diagnosed coefficients based on a local diffusion scheme. We also compared the ABL height of the sets E6 and H3.

With the results of these comparisons in mind, we want to return to our research questions. Comparison with ABL height measurements shows that the ABL height (question 1) archived in ERA-40 (E6) and the ABL height from the 3-hourly off-line non-local scheme (H3) are in reasonable agreement with the ABL height observations performed in Cabauw and during the FIFE campaign. The time resolution of 3 h makes the H3 ABL height more valuable than the 6-hourly E6 ABL height.

Vertical diffusion coefficients can be calculated accurately off-line (question 2a). The off-line diagnosed set of non-local diffusion coefficients (H3) is based on a parameterisation that is very similar to the parameterisation used in the ECMWF model to generate the archived diffusion coefficients (E3/E6). We find that the results are quite similar between the E3 and H3 case (both with 3-hourly time

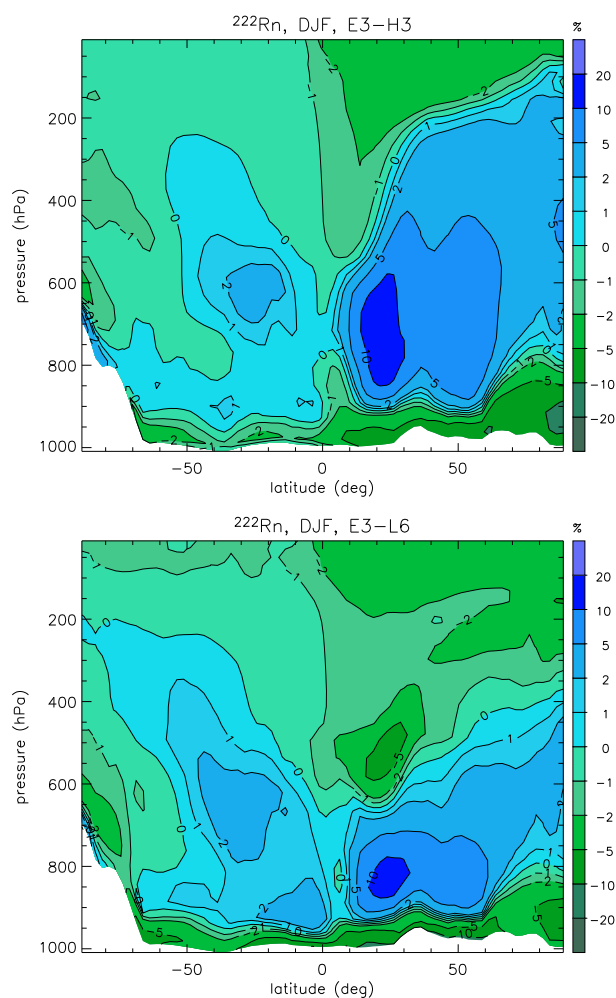


**Fig. 17.** Zonal mean relative difference (%) in  $^{222}\text{Rn}$  concentration between E3 and H3 (upper panel) and between E3 and L6 (lower panel) for DJF 1993.

resolution), and that the apparent difference can be attributed to small differences in the implementation of the parameterisation (different asymptotic mixing length, different stability functions, present or absent detrainment formulation). Hence the off-line diagnosis of diffusion coefficients reproduces quite well the archived diffusion coefficients.

The  $K_z$  values from the local scheme in the L6 case (question 2b) were sometimes quite different from the non-local scheme E6. Although the mean values of the diffusion coefficients in the lower troposphere were larger for the L6 case than for the E6 case, the instantaneous values led to smaller ABL transport. This could be attributed to the fact that the daytime  $^{222}\text{Rn}$  concentrations are not very sensitive to the much larger daytime L6 diffusion coefficients, while the smaller night time diffusion coefficients have a strong impact on the night concentration. Sometimes the  $K_z$  values of L6 and E6 were still surprisingly similar. This is due

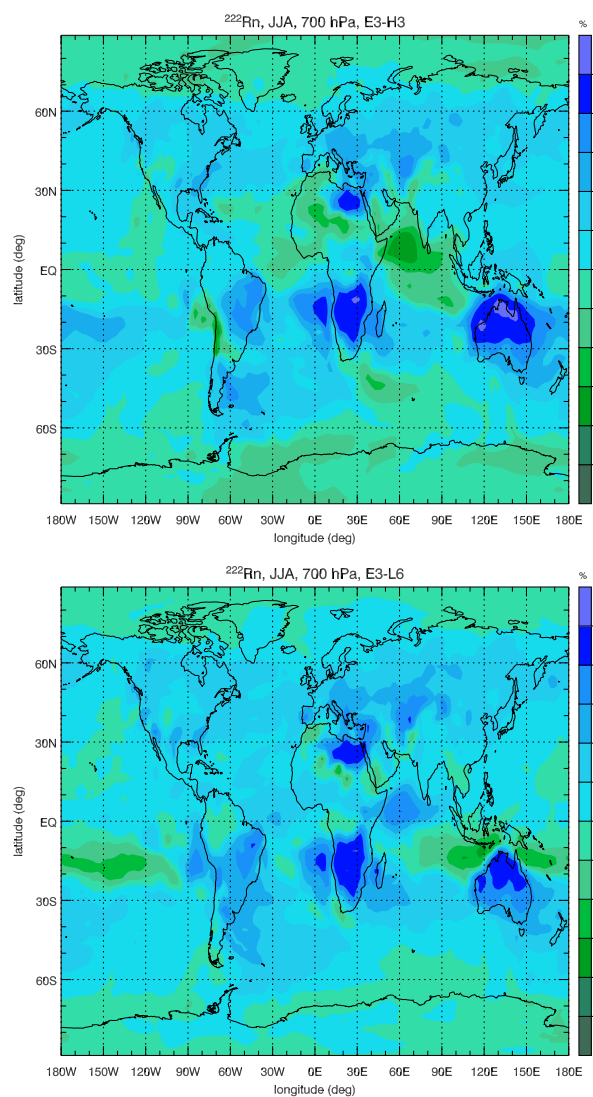


**Fig. 18.** The relative difference (%) in  $^{222}\text{Rn}$  concentration at 700 hPa between E3 and H3 (upper panel) and between E3 and L6 (lower panel) for DJF 1993.

to the fact that the underlying profiles of temperature, humidity and wind to drive the off-line L6 scheme are taken from the ECMWF-model.

Comparison of  $^{222}\text{Rn}$  simulations from the TM3 model with surface  $^{222}\text{Rn}$  observations in Freiburg, Schauinsland, Cincinnati, and Socorro shows that the 3-hourly E3 and H3 (question 3a) schemes perform better than the 6-hourly E6 and L6 schemes. Using the 3-hourly coefficients results in a better description of the daily cycle of the  $^{222}\text{Rn}$  concentration. This might have an impact on tracers that undergo fast photochemistry or are affected by dry deposition or vegetation.

It is also shown that using time-averaged diffusion coefficients (question 3b) can lead to time shifts of the daily cycle

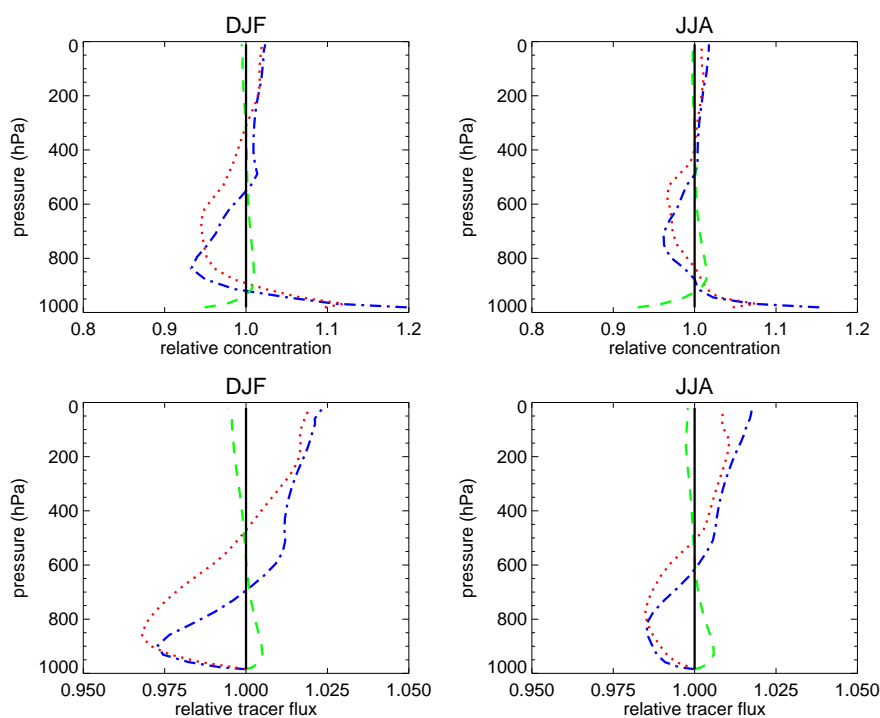


**Fig. 19.** Profiles of the global mean  $^{222}\text{Rn}$  concentration (upper panels) and profiles of the global mean net upward  $^{222}\text{Rn}$  flux (lower panels) are shown for DJF and JJA 1993. The concentration and flux of E3 (solid black), H3 (dotted red), E6 (dashed green), L6 (dot-dashed blue) are expressed with respect to the flux of E3.

of tracer concentrations and stronger vertical transport than instantaneous diffusion coefficients.

Finally, some recommendations can be formulated. First, using the E3 scheme resulted in higher  $^{222}\text{Rn}$  concentrations in the free troposphere than using the H3 scheme. The seasonal zonal and monthly mean  $^{222}\text{Rn}$  concentration can differ up to 10%. Earlier studies with the TM3 model suggested that vertical mixing was underestimated. As mentioned before, this difference can be partially attributed to the use of the detrainment formulation at the top of the ABL for the E3 case, a larger asymptotic mixing length, and differences in the stability functions. It would be therefore worthwhile making these changes in the off-line H3-scheme.

Secondly, the non-local schemes that are used here, do not contain a counter gradient term. Also here, it could be interesting to investigate whether including the counter gradient term could further improve the agreement with measurements.

Finally, the large discrepancy in  $^{222}\text{Rn}$  concentration between model and observations at some sites suggests that a more physical based emanation rate of  $^{222}\text{Rn}$  and perhaps a higher spatial resolution should be used.

*Acknowledgements.* This evaluation of diffusion coefficients would not have been possible without the atmospheric monitoring work of Mr. Sartorius from the Federal Office for Radiation Protection in Freiburg, Germany, who provided  $^{222}\text{Rn}$  data from the locations

Freiburg and Schauinsland. We thank H. Klein Baltink for the ABL height measurement data from Cabauw. ECMWF ERA-40 data used in this study have been provided by ECMWF. This work was supported by the Netherlands Organization for Scientific Research (NWO) and by the European Union under contract number EVK2-CT-2002-00170 (RETRO).

Edited by: F. J. Dentener

## References

- Allen, D. J., Rood, R. B., Thompson, A. M., and Hudson, R. D.: Three-dimensional radon  $^{222}$  calculations using assimilated meteorological data and a convective mixing algorithm, *J. Geophys. Res.*, D3, 101, 6871–6881, 1996.
- Balkanski, Y. J. and Jacob, D. J.: Transport of continental air to the subantarctic Indian Ocean, *Tellus B*, 42, 62–75, 1990.
- Beljaars, A. C. M. and Viterbo, P.: Role of the boundary layer in a numerical weather prediction model, in: *Clear and cloudy boundary layers*, edited by: Holtslag, A. A. M. and Duynkerke, P. G., pp. 287–304, NH-publishers, 1999.
- Bosveld, F., van Ulden, A., and Beljaars, A. C. M.: A comparison of ECMWF Re-Analysis data with fluxes and profiles observed in Cabauw, ECMWF Re-Analysis Project Report Series 8, ECMWF, Reading RG2 9AX, UK., 1999.
- Bregman, B., Segers, A., Krol, M., Meijer, E., and van Velthoven, P.: On the use of mass-conserving wind fields in chemistry trans-

- port models, *Atmos. Chem. Phys.*, 3, 447–457, 2003,  
**SRef-ID: 1680-7324/acp/2003-3-447.**
- Broecker, W. S., Li, Y. H., and Cromwell, J.: Radium-226 and radon-222 concentration in Atlantic and Pacific Oceans, *Science*, 158, 1307–1310, 1967.
- Brost, R. A. and Chatfield, R. B.: Transport of radon in a three-dimensional, subhemispheric model, *J. Geophys. Res.*, 94, 5095–5119, 1989.
- Dentener, F., Feichter, J., and Jeuken, A.: Simulation of the transport of  $^{222}\text{Rn}$  using on-line and off-line global models at different horizontal resolutions: a detailed comparison with measurements, *Tellus B*, 51, 573–602, 1999.
- Dentener, F., Peters, W., Krol, M., van Weele, M., Bergamaschi, P., and Lelieveld, J.: Interannual variability and trend of  $\text{CH}_4$  lifetime as measure for OH changes in the 1979–1993 time period, *J. Geophys. Res.*, 108, 4442, doi:10.1029/2002JD002916, 2003.
- Eloranta, E. W.: Boundary Layer Heights: LIDAR (FIFE). Data set., Available online [<http://www.daac.ornl.gov>] from Oak Ridge National Laboratory Distributed Active Archive Center, Oak Ridge, Tennessee, USA., also published in: *Collected Data of the First ISLSCP Field Experiment, Vol. 1: Surface Observations and Non-Image Data Sets*, edited by: Strelbel, D. E., Landis, D. R., Huemmrich, K. F., and Meeson, B. W., CD-ROM, National Aeronautics and Space Administration, Goddard Space Flight Center, Greenbelt, Maryland, USA., 1994.
- Feichter, J. and Crutzen, P. J.: Parameterization of vertical transport due to deep cumulus convection in a global transport model and its evaluation with  $^{222}\text{Rn}$  measurements, *Tellus B*, 42, 100–117, 1990.
- Gibson, J. K., Källberg, P., Uppala, S., Hernandez, A., Nomura, A., and Serrano, E.: ERA-15 description, ECMWF Re-Analysis Project Report Series 1, ECMWF, Reading RG2 9AX, UK., 1997.
- Gold, S., Barkhau, H. W., Shleien, B., and Kahn, B.: Measurements of naturally occurring radionuclides in air, in: *The Natural Radiation Environment*, edited by: Adams, J. A. S. and Lowder, W. M., pp. 369–382, University of Chicago Press, Chicago, Ill., 1964.
- Gregory, D., Morcrette, J.-J., Jakob, C., Beljaars, A. C. M., and Stockdale, T.: Revision of convection, radiation and cloud schemes in the ECMWF Integrated Forecasting System, *Q. J. R. Meteor. Soc.*, 126, 1685–1710, 2000.
- Heimann, M.: The global atmospheric tracer model TM2, Tech. Rep. 10, Deutsches Klimarechenzentrum, Hamburg, Germany, 1995.
- Holtstlag, A. A. M. and Boville, B. A.: Local versus nonlocal boundary-layer diffusion in a global climate model, *J. Climate*, 6, 1825–1842, 1993.
- Holtstlag, A. A. M., van Meijgaard, E., and de Rooy, W. C.: A comparison of boundary layer diffusion schemes in unstable conditions over land, *Boundary-Layer Meteorol.*, 76, 69–95, 1995.
- Houweling, A., Dentener, F., and Lelieveld, J.: The impact of non-methane hydrocarbon compounds on tropospheric photochemistry, *J. Geophys. Res.*, D9, 103, 10 673–10 696, 1998.
- Jacob, D. J. and Prather, M. J.: Radon-222 as a test of boundary layer convection in a general circulation model, *Tellus B*, 42, 117–134, 1990.
- Jacob, D. J., Prather, M. J., Rasch, P. J., Shia, R.-L., Balkanski, Y. L., Beagley, S. R., Bergmann, D. J., Blackshear, W. T., Brown, M., Chiba, M., Chipperfield, M. P., de Grandpré, J., Dignon, J. E., Feichter, J., Genthon, C., Grose, W. L., Kasibhatla, P. S., Köhler, I., Kritz, M. A., Law, K., Penner, J. E., Reeves, M. R. C. E., Rotman, D. A., Stockwell, D. Z., van Velthoven, P. F. J., Verver, G., Wild, O., Yang, H., and Zimmerman, P.: Evaluation and intercomparison of global transport models using  $^{222}\text{Rn}$  and other short-lived tracers, *J. Geophys. Res.*, D5, 102, 5953–5970, 1997.
- Jeuken, A.: Evaluation of chemistry and climate models using measurements and data assimilation, Ph.D. thesis, University of Technology Eindhoven, Eindhoven, The Netherlands, available at <http://alexandria.tue.nl/extra2/200001283.pdf>, 2000.
- Jeuken, A., Veeffkind, J. P., Dentener, F., Metzger, S., and Gonzales, C. R.: Simulation of the aerosol optical depth over Europe for August 1997 and a comparison with observations, *J. Geophys. Res.*, D22, 106, 28 295–28 311, 2001.
- Kritz, M. A., Roulley, J.-C. L., and Danielsen, E. F.: The China Clipper–fast advective transport of radon-rich air from the Asian boundary layer to the upper troposphere near California, *Tellus B*, 42, 46–61, 1990.
- Lambert, G., Polian, G., Sanak, J., Ardouin, B., Buisson, A., Jegou, A., and Roulley, J. C. L.: Cycle du radon et de ses descendants: application à l'étude des échanges troposphère-stratosphère, *Ann. Géophys.*, 4, 38, 497–531, 1982.
- Lee, H. N. and Larsen, R. J.: Vertical diffusion in the lower atmosphere using aircraft measurements of  $^{222}\text{Rn}$ , *J. Appl. Meteorol.*, 36, 1262–1270, 1997.
- Lelieveld, J. and Dentener, F.: What controls tropospheric ozone?, *J. Geophys. Res.*, D3, 105, 3531–3551, 2000.
- Liu, S. C., McAfee, J. R., and Cicerone, R. J.: Radon 222 and tropospheric vertical transport, *J. Geophys. Res.*, D5, 7291–7297, 1984.
- Louis, J.-F.: A parametric model of vertical eddy fluxes in the atmosphere, *Bound.-Layer Meteorol.*, 17, 187–202, 1979.
- Louis, J. F., Tiedtke, M., and Geleyn, J. F.: A short history of the operational PBL-parameterization at ECMWF, in: *Proceedings of ECMWF workshop on boundary layer parameterization*, November 1981, 59–79, ECMWF, Reading, England, 1982.
- Mahowald, N. M., Rasch, P. J., Eaton, B. E., Whittlestone, S., and Prinn, R.: Transport of  $^{222}\text{radon}$  to the remote troposphere using the Model of Atmospheric Transport and Chemistry and assimilated winds from ECMWF and the National Center for Environmental Prediction/NCAR, *J. Geophys. Res.*, D23, 102, 28 139–28 151, 1997.
- Nordeng, T. E.: Extended versions of the convective parameterization scheme at ECMWF and their impact on the mean and transient activity of the model in the tropics, Research Department Technical Memorandum 206, ECMWF, Reading RG2 9AX, UK., 1994.
- Olivie, D. J. L., van Velthoven, P. F. J., Beljaars, A., and Kelder, H. M.: Comparison between archived and off-line diagnosed convective mass fluxes in the chemistry transport model TM3, *J. Geophys. Res.*, D11, 109, D11 303, doi:10.1029/2003JD004036, 2004.
- Polian, G., Lambert, G., Ardouin, B., and Jegou, A.: Long-range transport of radon in subantarctic and antarctic areas, *Tellus B*, 38, 178–189, 1986.
- Russell, G. L. and Lerner, J. A.: A new finite-differencing scheme for the tracer transport equation, *J. Appl. Meteorol.*, 20, 1483–

- 1498, 1981.
- Sellers, P. J., Hall, F. G., Asrar, G., Strebel, D. E., and Murphy, R. E.: The First ISLSCP Field Experiment (FIFE), *Bull. Am. Meteor. Soc.*, 69, 22–27, 1988.
- Simmons, A. J. and Burridge, D. M.: An energy and angular-momentum conserving vertical finite-difference scheme and hybrid vertical coordinates, *Mon. Weather Rev.*, 109, 758–766, 1981.
- Simmons, A. J. and Gibson, J. K.: The ERA-40 project plan, ERA-40 Project Report Series 1, ECMWF, Reading RG2 9AX, UK., 2000.
- Stockwell, D. Z. and Chipperfield, M. P.: A tropospheric chemical-transport model: development and validation of the model transport schemes, *Q. J. R. Meteorol. Soc.*, 125, 1747–1783, 1999.
- Stockwell, D. Z., Kritz, M., Chipperfield, M. P., and Pyle, J. A.: Validation of an off-line three-dimensional chemical transport model using observed radon profiles 2. Model results, *J. Geophys. Res.*, D7, 103, 8433–8445, 1998.
- Tiedtke, M.: A comprehensive mass flux scheme for cumulus parameterization in large-scale models, *Mon. Weather Rev.*, 117, 1779–1800, 1989.
- Troen, I. and Mahrt, L.: A simple model of the atmospheric boundary layer; sensitivity to surface evaporation, *Bound.-Layer Meteor.*, 37, 129–148, 1986.
- Turekian, K. K., Nozaki, Y., and Benninger, L. K.: Geochemistry of atmospheric radon and radon products, *Ann. Rev. Earth Planet. Sci.*, 5, 227–255, 1977.
- Viterbo, P., Beljaars, A., Mahfouf, J.-F., and Teixeira, J.: The representation of soil moisture freezing and its impact on the stable boundary layer, *Q. J. R. Meteor. Soc.*, 125, 2401–2426, 1999.
- Vogelezang, D. H. P. and Holtslag, A. A. M.: Evaluation and model impacts of alternative boundary-layer height formulations, *Bound.-Layer Meteor.*, 81, 245–269, 1996.
- Wang, K.-Y., Pyle, J. A., Sanderson, M. G., and Bridgeman, C.: Implementation of a convective atmospheric boundary layer scheme in a tropospheric chemistry transport model, *J. Geophys. Res.*, D19, 104, 23 729–23 745, 1999.
- Wesely, M. L.: Boundary Layer Heights: SODAR (FIFE). Data set., Available online [<http://www.daac.ornl.gov>] from Oak Ridge National Laboratory Distributed Active Archive Center, Oak Ridge, Tennessee, USA, also published in: *Collected Data of the First ISLSCP Field Experiment, Vol. 1: Surface Observations and Non-Image Data Sets*, edited by: Strebel, D. E., Landis, D. R., Huemmrich, K. F., and Meeson, B. W., CD-ROM, National Aeronautics and Space Administration, Goddard Space Flight Center, Greenbelt, Maryland, USA, 1994.
- Wilkening, M. H.: Daily and annual courses of natural atmospheric radioactivity, *J. Geophys. Res.*, 64, 521–526, 1959.
- Wilkening, M. H. and Clements, W. E.: Radon 222 from the ocean surface, *J. Geophys. Res.*, 80, 3828–3830, 1975.
- Williamson, D. L., Kiehl, J. T., Ramanathan, V., Dickinson, R. E., and Hack, J. J.: Description of NCAR Community Climate Model (CCM1), NCAR Technical Note 285, NCAR, 1987.